CHALMERS
UNIVERSITY OF TECHNOLOGY

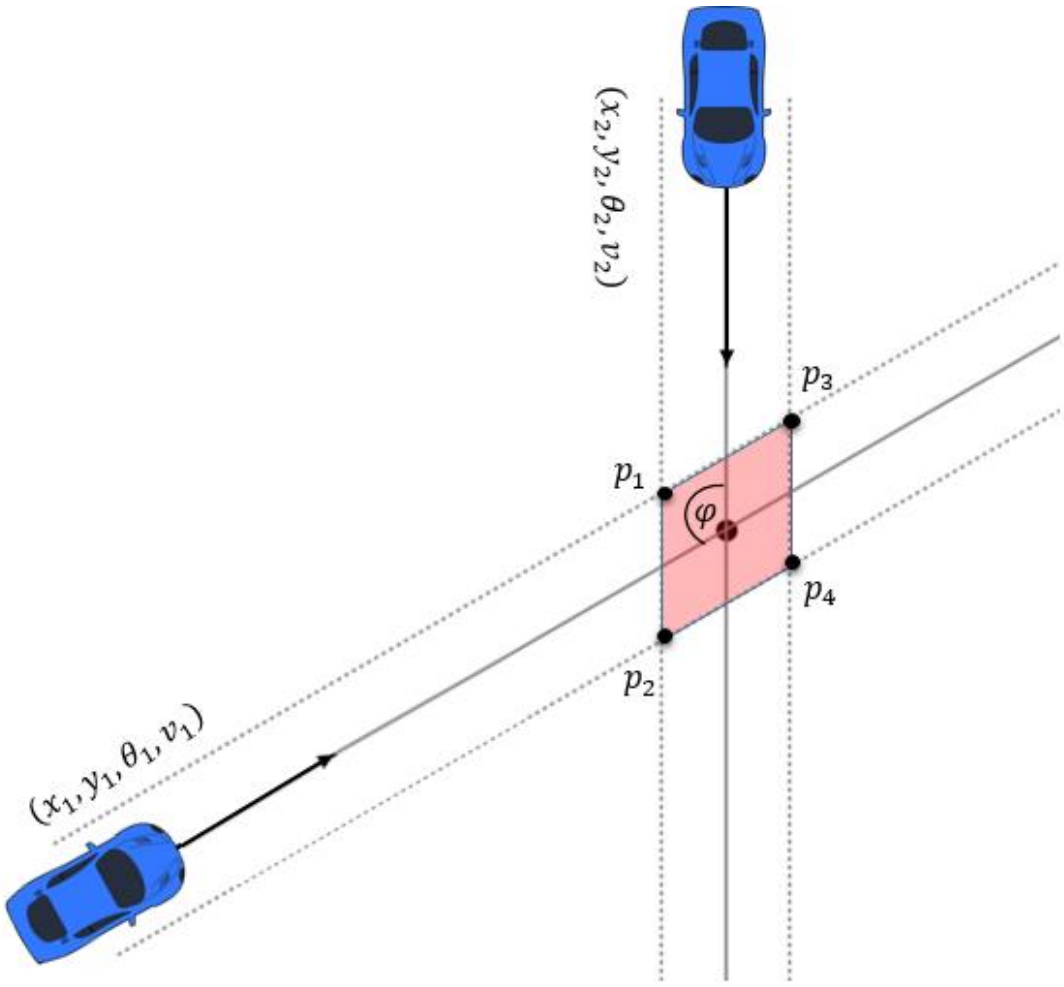

Last Point to React for Collision Avoidance in a Robotized Framework for Autonomous Driving Verification

Master's Thesis in Systems, Control and Mechatronics

Salma ABDELWAHAB

Department of Electrical Engineering
Division of Systems, Control and Mechatronics
CHALMERS UNIVERSITY OF TECHNOLOGY
Gothenburg, Sweden 2019
Master's Thesis 2019

MASTER'S THESIS 2019:EENX30

Last Point to React for Collision Avoidance in a Robotized Framework for Autonomous Driving Verification

Master's Thesis in Systems, Control and Mechatronics

Salma ABDELWAHAB

CHALMERS
UNIVERSITY OF TECHNOLOGY

Department of Electrical Engineering
Division of Systems, Control and Mechatronics
CHALMERS UNIVERSITY OF TECHNOLOGY
Gothenburg, Sweden 2019

Last Point to React for Collision Avoidance in a Robotized Framework for Autonomous Driving Verification.

Master's Thesis in Systems, Control and Mechatronics

Salma ABDELWAHAB

Supervisor: Angel Molina Acosta, Volvo Car Corporation
Supervisor/Examiner: Jonas Sjöberg, Chalmers University of Technology

Master's Thesis 2019:EENX30
Department of Electrical Engineering
Division of Systems, Control and Mechatronics
CHALMERS UNIVERSITY OF TECHNOLOGY
SE-412 96 Gothenburg
Sweden
Telephone: + 46 (0)31-772 1000

Cover:
Schematic illustration of the modelling of the angled collision scenarios considered in this thesis work, where φ is the intersection angle. The red area corresponds to the zone where collisions may occur, defined with p_1, p_2, p_3, and p_4.

Gothenburg, Sweden, 2019

Last Point to React for Collision Avoidance in a Robotized Framework for Autonomous Driving Verification

Master's thesis in Systems, Control and Mechatronics

Salma ABDELWAHAB
Department of Electrical Engineering
Division of Systems, Control and Mechatronics
CHALMERS UNIVERSITY OF TECHNOLOGY

Abstract

Autonomous driving has been lately the focus of the automotive industry for its potential to improve traffic safety. In order to commercialize this promising technology, numerous tests must be carried out to guarantee its reliability. This master thesis proposes a supervisor module for an autonomous driving test framework ensuring the safe execution of the test case when emergency situations arise by forcing the test vehicles to follow safe trajectories.

We have been focusing on a specific vehicle in the loop (VIL) test environment comprised of a robotized framework where test vehicles are equipped with a specialized driving robot that can actuate the throttle and brake pedals as well as the steering wheel. Over a 4G network, a server sends trajectories to the target vehicles which they follow to recreate a desired traffic scenario. All vehicles on the test track communicate their current states with the server to ensure closed-loop control.

Hence, the supervision and control strategy is developed based on a geometrical approach considering the vehicle's motion limitations. According to the vehicles' states at a given time instant, we estimate future trajectories of the vehicles, predict potential collisions, and generate steering and braking maneuver-based trajectories for collision avoidance. As our aim is to only intervene in case of emergency, we compare the activation time of each proposed maneuver in order to define the last point to react for collision avoidance.

A set of experiments for speeds between 20kph and 60kph were performed on a test vehicle equipped with the driving robot that will be used in the previously-mentioned framework. The results have revealed that, for the majority of the scenarios investigated in this thesis work, the last point to react is 1 second before collision. The driving robot is effectively able to follow the generated trajectories, even for cases that require high levels of lateral or longitudinal acceleration. However, analysing less conservative safety maneuvers could significantly improve the intervention time.

Key words: Collision Avoidance, Active Safety, Autonomous Driving Verification, VIL "Vehicle In the Loop", Robotized Framework, Last Point to Steer, Last Point to Brake, Last Point to React

Acknowledgments

I would first like to express my sincere gratitude to Siddhant Gupta and Francesco Costagliola at Volvo Cars Corporation for providing me with this Master's Thesis opportunity, and for their significant support and guidance which they have offered to me throughout this journey.

I would also like to thank my supervisor Angel Molina Acosta at Volvo Cars Corporation. The door to Angel's office was always open whenever I ran into a trouble spot or had a concern about my research. He consistently steered me in the right direction whenever he thought I needed it.

A very special gratitude goes out to Daniel Johansson, doing his Master's Thesis on the same project, for his continuous support, valuable help and cooperation.

I am very thankful to the Virtual Car team and the Robot team at Volvo Cars Corporation for their encouragement, their timely technical support, and not to forget the excellent working atmosphere.

I owe my deep gratitude to my academic supervisor Professor Jonas Sjöberg at Chalmers University of Technology for giving me all support and guidance which made me complete the project duly, despite his very busy schedule.

I would not forget to remember Professor Claudine Gehin at INSA Lyon and Sir Andreas Eriksson at Chalmers University of Technology who ensured that my academic exchange ran smoothly.

I heartily thank my eternal cheerleaders, comprised of my family and my friends who have provided me with moral and emotional support along the way.

And finally, to my father Tarek Elwakil: because I owe it all to you. Many thanks!

Salma Abdelwahab
Gothenburg, June 2019

Contents

Notations

Abbreviations

AD	**A**utonomous **D**riving
ADAS	**A**dvanced **D**river-**A**ssistance **S**ystems
APF	**A**rtificial **P**otential **F**ield
AS	**A**ctive **S**afety
HIL	**H**ardware **I**n the **L**oop
ORCA	**O**ptimal **R**eciprocal **C**ollision **A**voidance
MIL	**M**odel **I**n the **L**oop
MPC	**M**odel **P**redictive **C**ontrol
PIL	**P**rocessor **I**n the **L**oop
RRT	**R**apidly-exploring **R**andom **T**ree
SAE	**S**ociety of **A**utomotive **E**ngineers
SIL	**S**oftware **I**n the **L**oop
TTC	**T**ime **T**o **C**ollision
VIL	**V**ehicle **I**n the **L**oop
VUT	**V**ehicle **U**nder **T**est

Symbols

φ	collision angle
θ_i	heading angle of vehicle i
d	lateral displacement
dR	safe margin width
i	vehicle index
k	trajectory node index
L_{bi}	braking distance for vehicle i
L_{si}	steering distance for vehicle i
$\mathbb{N}$	set of natural number
O_i	occupancy interval for vehicle i
p_1	cartesian point representing the 1st corner of the collision area
p_2	cartesian point representing the 2nd corner of the collision area
p_3	cartesian point representing the 3rd corner of the collision area
p_4	cartesian point representing the 4th corner of the collision area
p_c	cartesian point representing the collision center
p_{b_i}	cartesian point representing the last point to brake for vehicle i
p_{t_i}	cartesian point representing a tangent point to the steering maneuver
p_{s_i}	cartesian point representing the last point to steer for vehicle i
p_{st_i}	cartesian point representing the stop point for vehicle i
$\mathbb{R}^+$	set of positive real numbers
R_i	steering radius for vehicle i
S_i	steering maneuver center for vehicle i
t_s	sampling time
v_i	velocity of vehicle i
x_c	x coordinate of p_c
x_i	x coordinate of vehicle i
y_c	y coordinate of p_c
y_i	y coordinate of vehicle i

List of figures

1 Introduction

Volvo Cars believes that autonomous drive technology will have a significant impact on people's lives and will be an important step towards more sustainable and safer mobility. In the fall of 2018, they revealed Volvo Cars' 360c autonomous concept, see Figure 1.1, with the vision of imagining a world in which we can travel long distances without the need to go to airports and instead we could ride the new Volvo 360c self-driving car.

Figure 1.1: *Volvo Cars' 360c autonomous concept. (Source: Volvo Cars).*

Despite of all the active safety (AS) and advanced driver-assistance systems (ADAS) installed in vehicles nowadays, e.g. ABS "Anti-lock Braking System", ESC "Electronic Stability Control", EBS "Emergency Braking System", ACC "Adaptive Cruise Control", and others, over 3 700 people pass away on the world's road every day and tens of millions of people are injured or disabled every year according to WHO's infographics on road safety [1]. Another serious fact is that 90% of traffic accidents in Europe are due to human error, according to the European Commission of Mobility and Transport [2]. Many benefits are anticipated to arise from the introduction of highly automated driving technology. Self-driving vehicles, with the help of advanced equipped sensors that can analyse the surrounding environment and adapt its navigation according to the traffic conditions, will ensure the removal of human error and will provide reduced congestion, increased accessibility to transport, and less impact on the environment.

Throughout the history of automotive industry, Volvo Cars has always been distinguished for their revolutionary technologies in road safety and mobility, starting with the three-

point seatbelt in 1959 which is today standard in all vehicles [3]. Fulfilling their current mission that no one should be seriously injured or killed in a new Volvo Car by 2020, Volvo Cars along with other automotive partners are investing significant resources on road active safety by developing a unique platform for test and research on autonomous driving (AD). The long term goal of this research project, that they have called CHRONOS, is to test and validate autonomous driving (AD) functionalities in complex traffic scenarios with up to hundred test objects [4].

1.1 Background

This thesis work contributes to the area of autonomous driving verification, precisely to the research done at Volvo Cars Corporation and the CHRONOS project. The society of Automotive Engineers (SAE) International has recently published a chart, see Figure 1.2, to clarify its J3016 standard in order to avoid any ambiguity on driving automation levels. The J3016 standard classifies vehicles with autonomous driving (AD) functionalities into six levels of driving automation, going from SAE Level 0 (no automation) to SAE Level 5 (full automation). Volvo Cars is now focusing important resources on developing and producing highly safe cars with functionalities that correspond to SAE level 4 and 5.

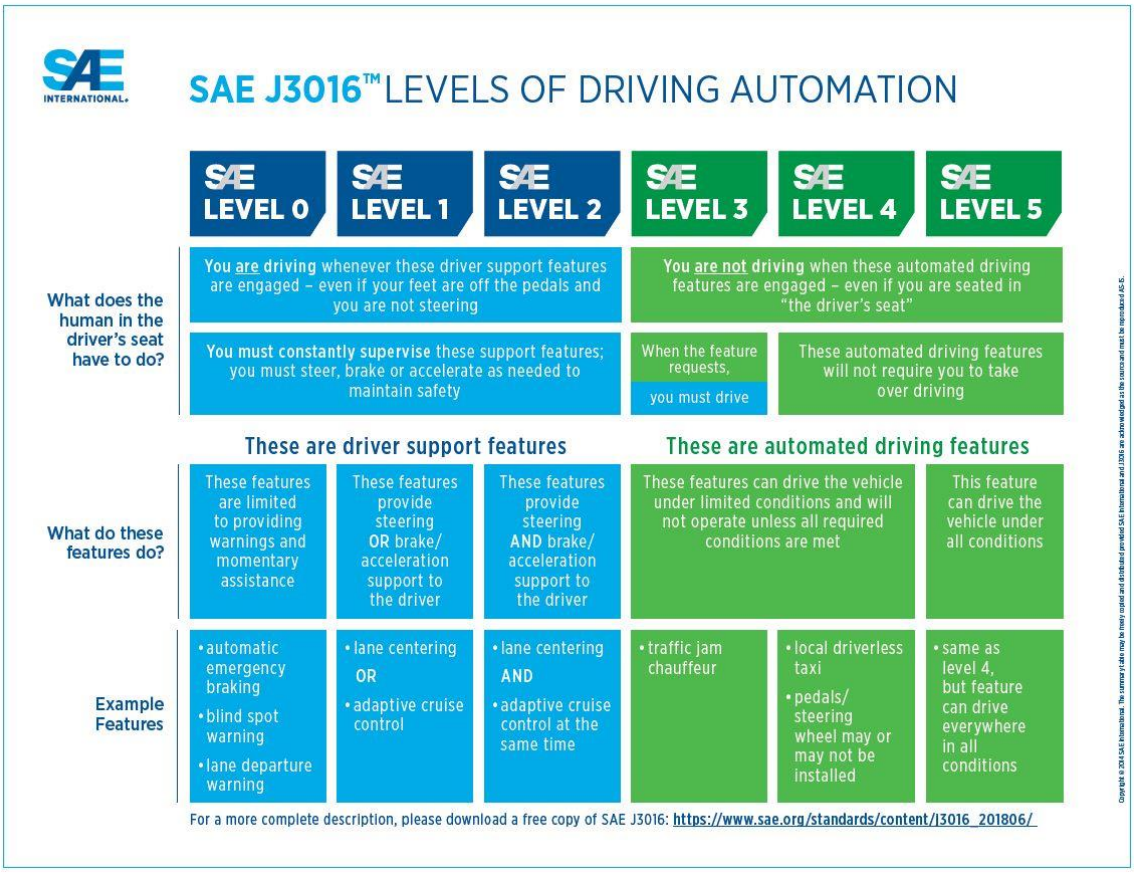

Figure 1.2: *SAE International visual chart (Source: SAE).*

In order to commercialize those vehicles, a sophisticated test and validation system is required. Volvo cars follows the ISO 26262 V-Cycle for developing safe systems for autonomous driving (AD) functions. ISO 26262 specifies how to test and validate the software and the hardware safety requirements in a systematic manner including model-

in-the-loop (MIL), software-in-the-loop (SIL), processor-in-the-loop (PIL), and hardware-in-the-loop (HIL) tests before running real-world tests which are also known as vehicle-in-the-loop (VIL) tests, see Figure 1.3.

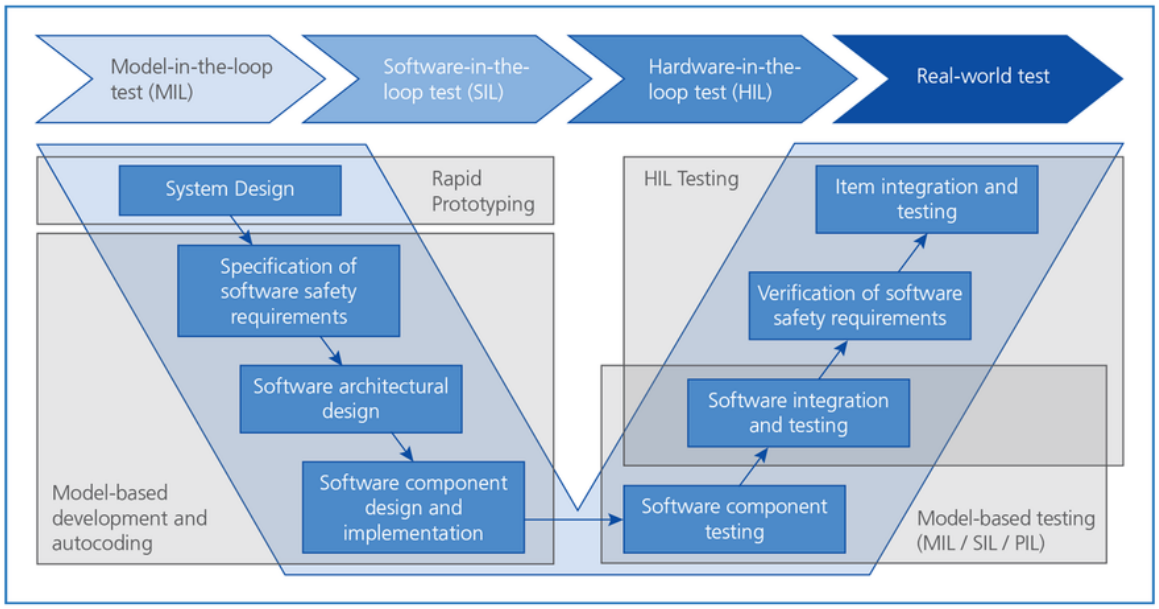

Figure 1.3: *ISO 26262 software safety requirements verification (Source: dSPACE).*

CHRONOS, the previously mentioned research project for autonomous driving (AD) verification, is a robotized framework for vehicle-in-the-loop (VIL) tests which are carried out on a test track with all sensors and software installed in the vehicle under test (VUT). The surrounding environment is comprised of real target vehicles, dynamic soft targets, and virtual target objects in order to recreate a traffic scenario. Real vehicles are equipped with driving robots that are capable of applying accurate torque to the vehicle's steering system and actuate the throttle and brake pedals, see Figure 1.4. Thanks to these robots, the target vehicles navigate on the test track according to a predefined test scenario with an accuracy that no human driver can achieve. Moreover, the vehicle under test (VUT) is equipped with the same customized driving robot to take full control of the vehicle in case of emergency.

Figure 1.4: *Steering Robot on the left, and Pedals Robot on the right.*

Over a 4G network, a central server communicates with all test objects defined in the test scenario including the vehicle under test (VUT) in order to ensure a closed-loop control, see Figure 1.5. The main role of the server is to handle test execution by generating trajectories corresponding to the chosen test scenario, and to guarantee safe execution

by generating backup collision-free trajectories that the test objects should follow in case of emergency. Therefore, a supervisor module is sought to be implemented in the central server to monitor the test objects and detect if dangerous situations arise such as potential collisions, one or more target objects diverting from their intended trajectory, loss of communication, etc. Only when the situation becomes highly dangerous, an emergency action should be performed to safely abort the test.

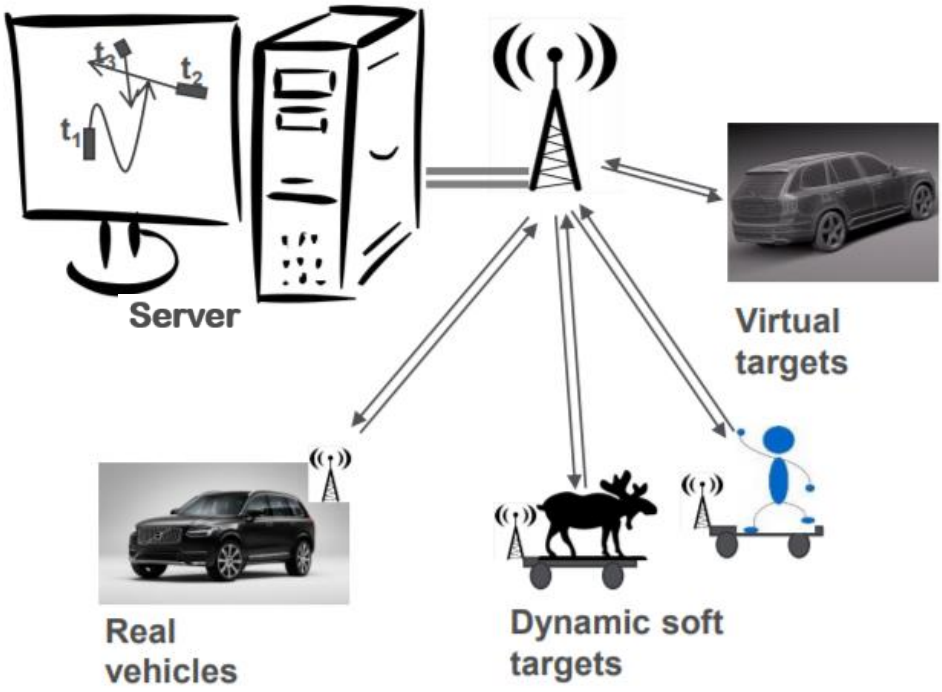

***Figure 1.5**: Robotized Test Framework.*

1.2 Literature Review

An in-depth study was carried out to position the current state of collision threat assessment strategies and dynamic path planning algorithms for collision avoidance.

Collision threat assessment algorithms can be classified into two big families: deterministic and probabilistic approaches. A deterministic approach, is based on calculating the possibility of collision as a binary prediction regarding many threat measures such as time to collision (TTC), time to brake, time to steer, headway time, etc. Glaser and Vanholme [5] use two threat measures which are time to collision (TTC) and inter-vehicular time as parameters to predict future potential collisions between two vehicles in a specific traffic situation. Shah [6] uses time to steer and time to brake to develop a rear-end collision avoidance system. Such deterministic approaches have the advantage of being simple and computationally efficient, but they do not model uncertainties in their input data since they assume a constant input; e.g. constant yaw rate and constant acceleration. To cope with this problem, probabilistic approaches [7][8][9] have been proposed describing spatial and temporal relationships between vehicles and incorporating the uncertainties since yaw rate and acceleration are highly unlikely to

remain constant in real traffic situation. The primordial weakness of this probabilistic approach is its computational cost and fast expansion of the threat set leading to unfeasible solution for collision avoidance [10].

A significant amount of research has been conducted on path planning, originally for robotic applications and, nowadays, for vehicles. Dynamic path planning algorithms for collision avoidance usually have a desired goal position in a known or semi-known environment which they try to reach without colliding with the surrounding static or moving objects but do not predict potential collisions; e.g. dynamic A* [11], rapidly-exploring random tree (RRT)[12], artificial potential fields (APF)[13], and others. Recently, optimal control[14] and model predictive control[15][16] (MPC) have been used for dynamic path planning and have revealed excellent results for collision avoidance in overtaking scenarios [15] or intersection scenarios[16] thanks to its prediction capabilities over a long time horizon. In [14] [15] [16], the calculations are quite heavy due to online optimization making its real-time implementation a burden. Equally promising, optimal reciprocal collision avoidance (ORCA) [17] algorithm generates collision-free trajectories for multiple agents environment in a cooperative manner based on the concept of velocity obstacles to predict and avoid collisions. Optimal reciprocal collision avoidance (ORCA) is studied by Daniel Johansson in another thesis work [18] run in parallel to this thesis at Volvo Cars Corporation. Yet, when to trigger the collision-free trajectories prescribed by the ORCA algorithm remains an open question.

1.3 Motivation

According to the literature review, it is notable that there is a dearth of research on combining collision threat assessment algorithms with dynamic path planning algorithms for collision avoidance. The purpose of the research carried out in this thesis is not only to predict potential collisions and generate collision-free trajectories but also to formulate what it is an emergency situation. The main motivation is to investigate how the last point to react for collision avoidance can be defined in a vehicle in the loop (VIL) test framework for autonomous driving (AD) verification, while ensuring that the safe trajectories are not triggered too soon so that the AD functionalities can be tested sufficiently close to a collision.

1.4 Problem Formulation

We consider the problem of monitoring two vehicles, a target vehicle and a vehicle under test (VUT), in angled collision scenarios discarding front-end and rear-end collision scenarios. Those two specific cases require a separate analysis that is not conducted in this thesis.

We have assumed that vehicles drive at constant speed and with a fixed heading angle for the sake of simplifying the estimation of their future trajectories. Nevertheless, the test track area is considered as an open space to eliminate any road map constraints.

The test scenario is parameterized with an angle $\varphi \in]\, 0°, 180° \,[$, which is the intersection angle between the vehicles' estimated trajectories. Vehicles considered in the study case are updating the central server with their current states: x_i and y_i coordinates with respect to a common fixed coordinate system, heading angle θ_i, and velocity v_i. Safe

trajectories are thus sought such that a collision within the zone defined with p_1, p_2, p_3 and p_4 is avoided, see Figure 1.6. It should be noted that those safe trajectories are not meant to be used to achieve autonomous driving.

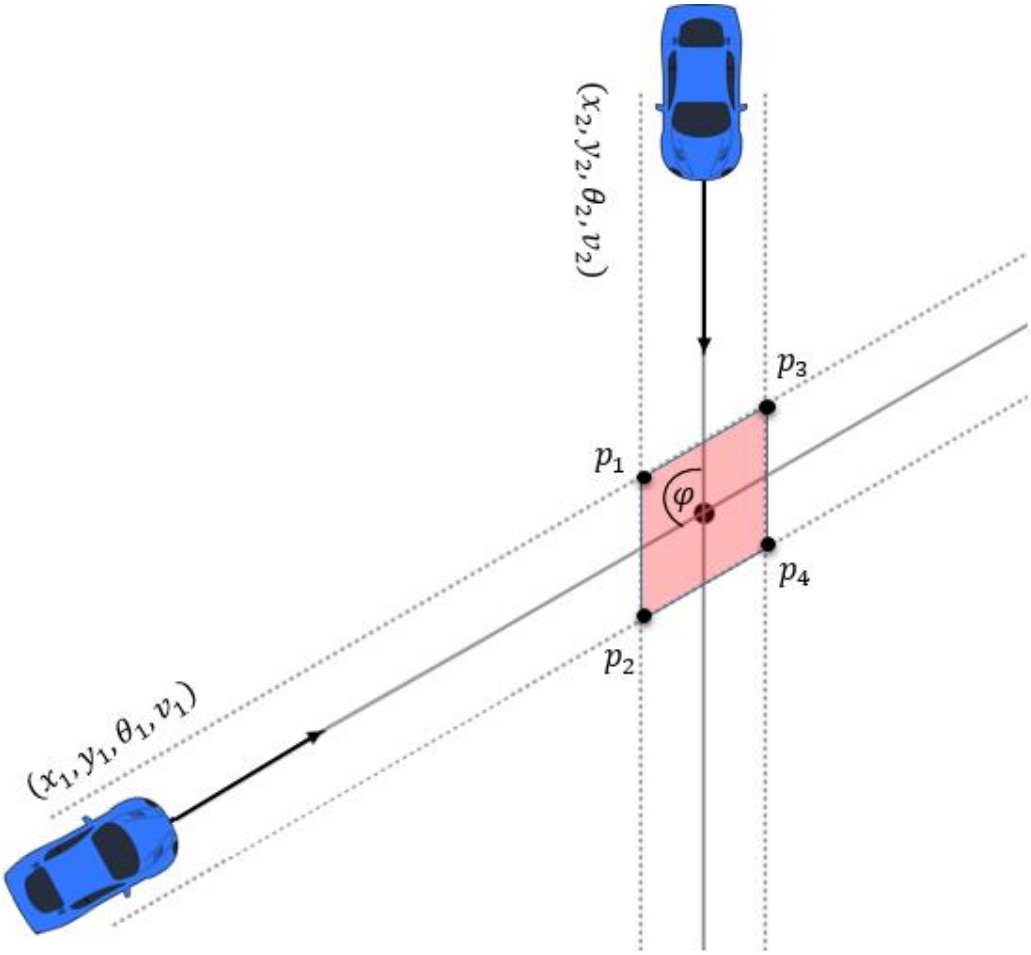

Figure 1.6: *Schematic illustration of the modelling of the angled collision scenarios considered in this thesis work.*

1.5 Contributions

A supervisor control module is proposed for securitizing vehicle in the loop (VIL) robotized tests for autonomous driving verification. The supervisor monitors the test objects and guarantee safe exits for the vehicles included in the test case when it assesses the situation as an emergency thanks to the last point to react approach introduced in this thesis work.

1.6 Outline

The remainder of this thesis report is structured as follows. In Chapter 2, the collision detection strategy is described. The proposed algorithm includes future trajectories'

estimation, intersection verification, collision area identification, and collision threat assessment.

Chapter 3 details how safety maneuvers for collision-free path planning are developed based on a geometrical approach and a desired vehicle motion. The designed maneuvers are evaluated based on their last point to react and the results are presented at the end of chapter.

In Chapter 4, the functional architecture of the supervisor module is covered, ranging from receiving vehicles' current states from the central server to the performance of an emergency action for collision avoidance. Suitable simulations are conducted for performance analysis and the benchmark behaviour is given at the end of chapter.

Chapter 5 is dedicated to the experimental validation. We bring up experimental results and simultaneously discuss and present solutions to overcome problems identified in the proposed approach.

Finally, Chapter 6 concludes the thesis work, summarises the results and initiates possible further work.

2 Collision Detection

In this Chapter, we detail the deterministic approach used to develop the collision detection module which is a component of the supervisor module to be incorporated in the central server. The algorithm firstly estimates vehicles' future paths based on their current states. Afterwards, it assesses the possibility of potential collisions by evaluating the occupation time of each vehicle in the identified collision area.

2.1 Future Trajectory Estimation

Consider two vehicles included in the test scenario, monitored by the supervisor module and updating the central server with their current states: x_i and y_i coordinates, heading θ_i, and speed v_i as shown in Figure 2.1. For each vehicle i, we assume that:

- Vehicles drive straight with constant heading
- Vehicles keep constant speed

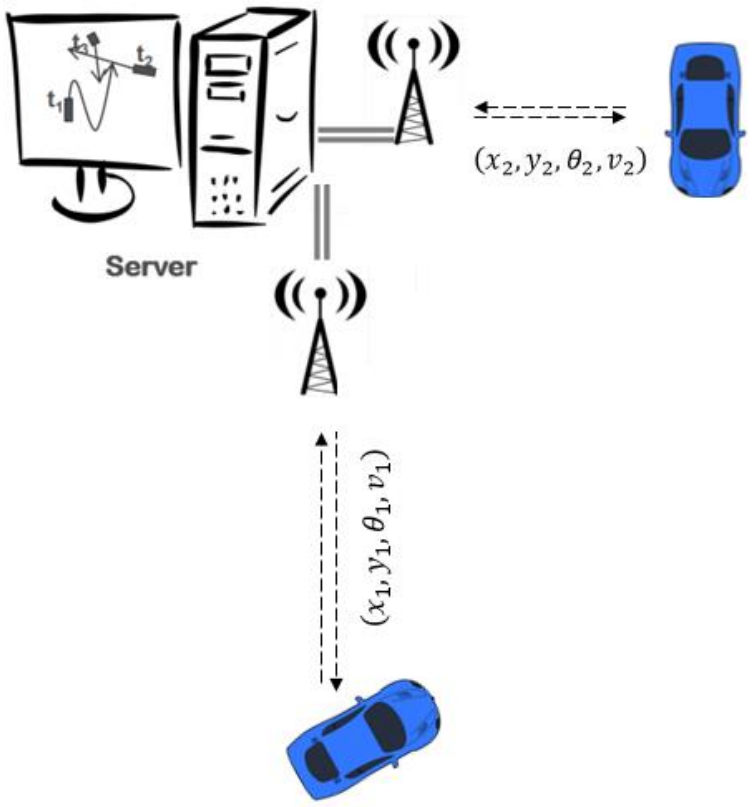

Figure 2.1: *Illustration of a given state of the running test scenario.*

Scenarios where the acceleration and yaw rate might change along the vehicles' paths are not considered in this study as this would require a more elaborated approach for path estimation which will be computationally expensive. We seek to implement an algorithm with low computational demands to address the problem defined in this thesis.

Spatial expressions are needed to describe the location of the vehicles along the estimated path. As a consequence of the assumptions stated before, a linear extrapolation method can be applied to express the vehicles' future paths, see Figure 2.2. To put it differently, we are looking to define the straight line that passes through the current position (x_{i_k}, y_{i_k}) and a future position $(x_{i_{k+\Delta t}}, y_{I_{k+\Delta t}})$ determined with 2.1 and 2.2. Since the future position is only used to find the sought spatial function, Δt could take any value.

$$x_{i_{k+\Delta t}} = x_{i_k} + v_i \Delta t \cos\theta_i \qquad \forall\, i \in \{1,2\} \tag{2.1}$$

$$y_{i_{k+\Delta t}} = y_{i_k} + v_i \Delta t \sin\theta_i \qquad \forall\, i \in \{1,2\} \tag{2.2}$$

Therefore, vehicles' estimated paths are described by the function $y_i(x_i)$ that can be formally written as:

$$y_i = \frac{y_{i_{k+\Delta t}} - y_{i_k}}{x_{i_{k+\Delta t}} - x_{i_k}} (x_i - x_{i_k}) + y_{i_k} \tag{2.3}$$

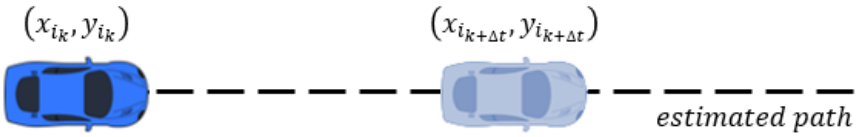

Figure 2.2: *Illustration of linear extrapolation using a current position (x_{i_k}, y_{i_k}) and a future position $(x_{i_{k+\Delta t}}, y_{I_{k+\Delta t}})$to find the estimated path.*

2.2 Intersection Verification

In order to verify if a collision may occur or not, we need to verify if the estimated trajectories are intersecting in the future, see Scenario 1 in Figure 2.3. On the ground that vehicles future trajectories are straight lines, the intersection point can be found by solving the following system of equations derived from (2.3):

$$\begin{cases} a_1 x + b_1 y = c_1 \\ a_2 x + b_2 y = c_2 \end{cases} \tag{2.4}$$

(2.5)

The linear system of equations comprised of (2.4) and (2.5) is represented in matrix format as shown below:

$$\begin{bmatrix} a_1 & b_1 \\ a_2 & b_2 \end{bmatrix} \begin{bmatrix} x \\ y \end{bmatrix} = \begin{bmatrix} c_1 \\ c_2 \end{bmatrix} \tag{2.6}$$

The solution is thus obtained by inverting the matrix. If the matrix is non-invertible, this means that the running test scenario is safe, see Scenario 2 in Figure 2.3. Otherwise, the intersection point "p_c" is trivial:

$$x_c = \frac{c_1 b_2 - b_1 c_2}{a_1 b_2 - b_1 a_2} \tag{2.7}$$

$$y_c = \frac{a_1 c_2 - c_1 a_2}{a_1 b_2 - b_1 a_2} \tag{2.8}$$

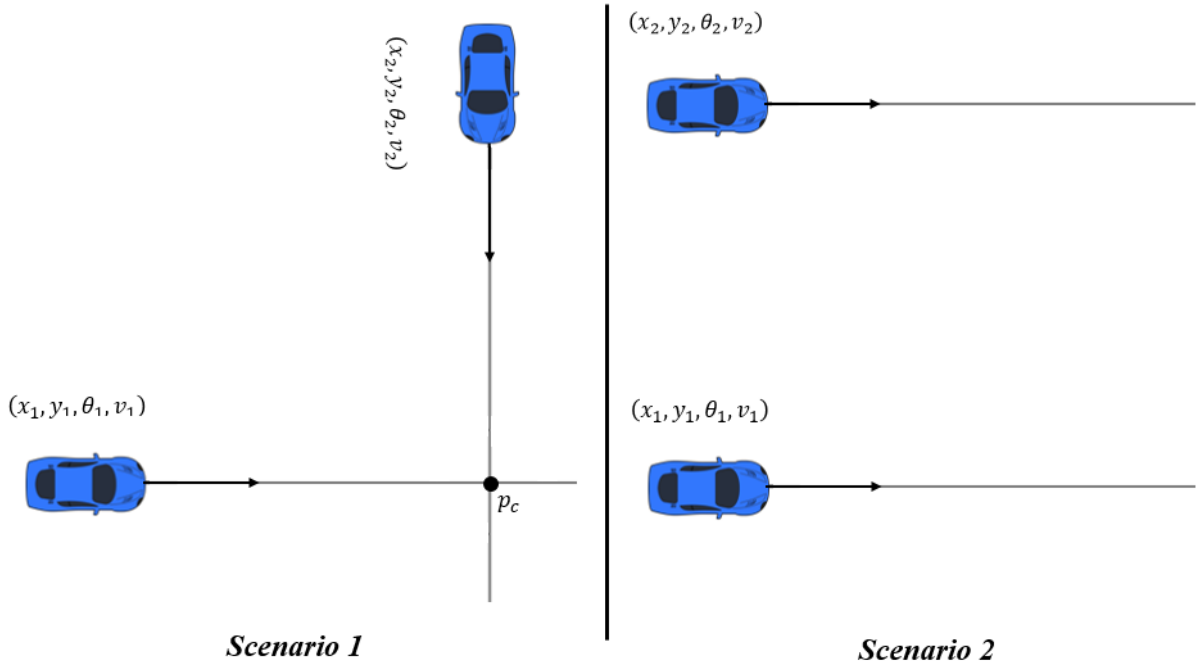

Figure 2.3: *Illustration of future trajectory estimation for two different scenarios.*

2.3 Collision Area Identification

The collision area is defined with p_1, p_2, p_3 and p_4 based on the intersection between the safe margins, see Figure 2.3. Safe margins are placed 1m away from each vehicle side in order to account for any path following error, further discussed in Chapter 5. This defined zone is thus the dangerous area were collisions may occur if the vehicles travel according to the prediction.

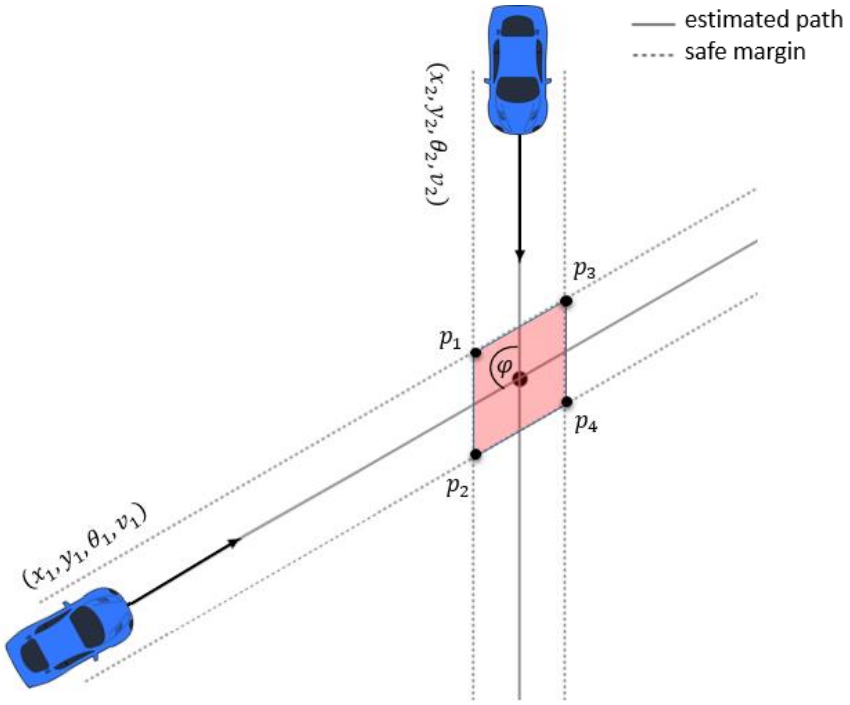

Figure 2.4: *Illustration of the collision area represented by the red zone.*

2.4 Collision Threat Assessment

Collisions are absolutely occurring if both vehicles at a time reside within the pre-defined collision area. Therefore, we chose the occupancy interval as a threat metric. We assume that at time $t = t_0$, vehicles are at the exact given position shared with the supervisor module. For each vehicle i we define the occupancy interval as in (2.9) and illustrated in Figure 2.5.

$$O_i(t) = \{t \in [t_{i_1}, t_{i_2}]\} \qquad \forall\, i \in \{1,2\} \tag{2.9}$$

We precise that "t_{i_1}" corresponds to the time at which the front bumper of the vehicle enters the collision area and "t_{i_2}" corresponds to the time at which the rear bumper leaves the collision area. Therefore, the length of the vehicle should be a priori known in order to calculate the distance travelled from the vehicle's current position to where the front bumper crosses $\overline{p_1 p_2}$ and to where the rear bumper crosses $\overline{p_3 p_4}$. On account of that vehicles keep constant speed, "t_{i_1}" and "t_{i_2}" are easily calculated.

As a result, we express the collision threat metric with the following equation:

$$Threat = O_1(t) \cap O_2(t) \tag{2.10}$$

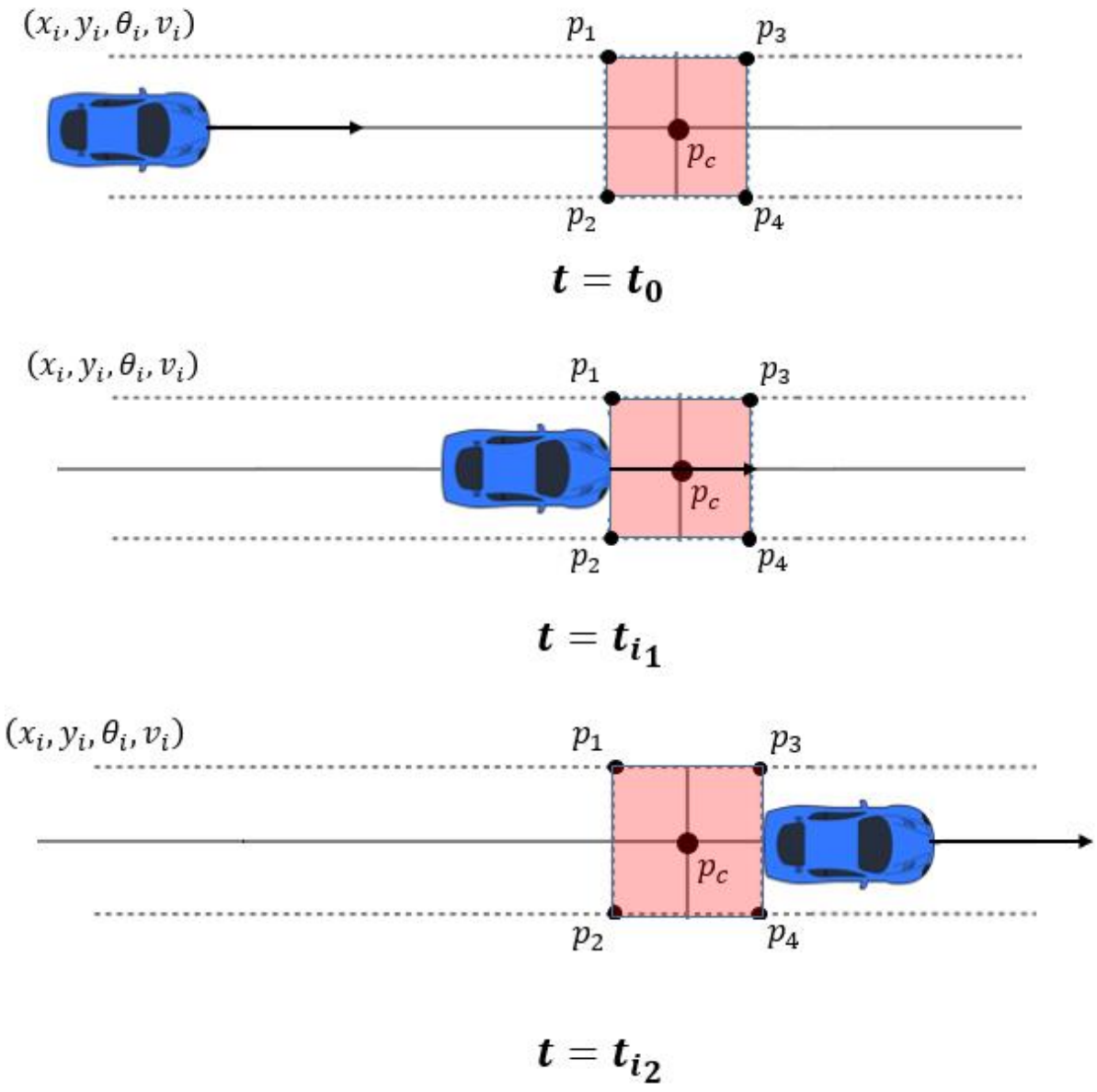

Figure 2.5: *Illustration of vehicle temporal position at different critical times.*

3 Safety Maneuvers

In this chapter, we present different evasive emergency maneuvers for angled collision avoidance inspired by an autonomous driving system designed to avoid rear-end collisions [6]. A geometrical approach was seen to satisfy the requirements of dynamic path planning and low computational power which are aimed to be fulfilled in this thesis work. First, we elaborate in the following sections how the evasive maneuvers were developed and how the last point to react is defined. The last point to react refers to the last point to steer or to brake; it depends on the selected driving action to avoid collision. After the vehicle crosses this point, no feasible solution can be found for collision avoidance in view of the physical limits of the vehicles. Afterwards, the generation process of collision-free trajectories is explained. At last, we evaluate and compare the performance of each safety maneuver.

3.1 Steer – Steer Safety Maneuver

3.1.1 Related Work

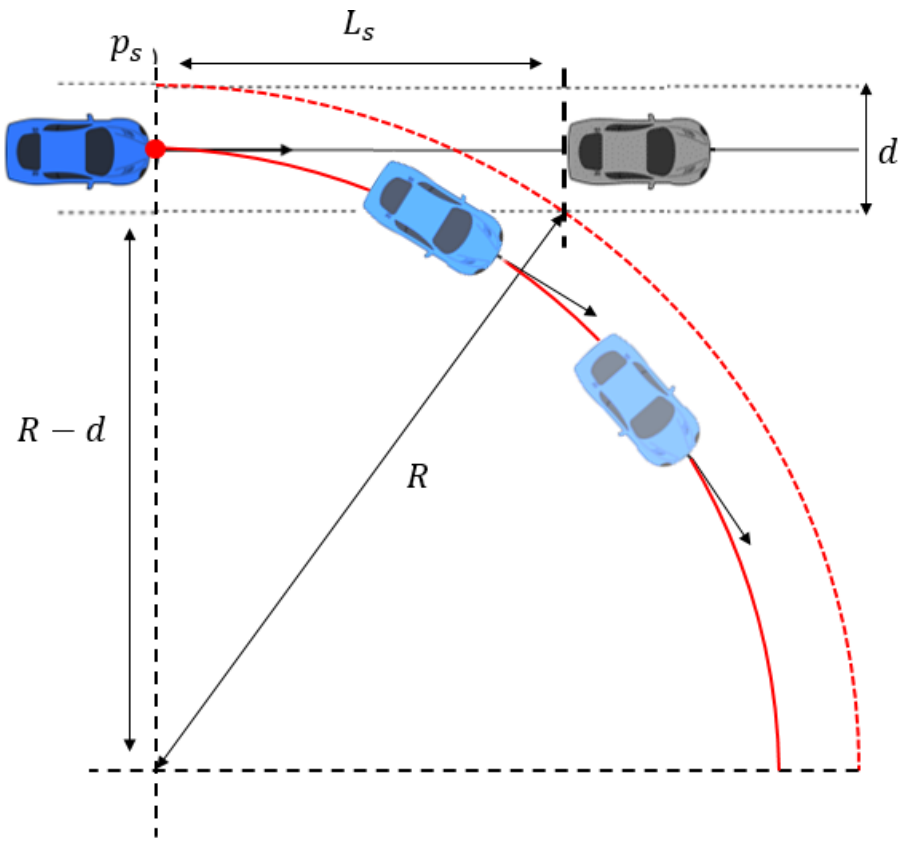

Figure 3.1: *Illustration of autonomous rear-end collision avoidance by steering away from the obstacle.*
The blue car represents the controlled object and in contrast the grey car represents the obstacle.

Steering was used in [6] for rear-end collision avoidance. In Figure 3.1, we illustrate the studied scenario where the blue car represents the controlled vehicle and the grey car is at standstill. "L_s" is the distance along the road required for the blue car to achieve a lateral displacement "d" when it drives on a circular path of radius "R". The steering radius "R" is defined according to the desired lateral acceleration and the forward speed of the vehicle, which is assumed to remain constant. On account of "R" and "d", the required distance "L_s" is calculated designating the last point to steer "p_s". Therefore, the blue car must start steering where it is at least "L_s" behind the grey car to avoid collision.

3.1.2 Approach

First of all, we have investigated how to apply the last point to steer concept described in the last section to angled collision avoidance. The geometrical approach illustrated in Figure 3.1 needed to be adapted to angled collision scenarios taking into account that both vehicles can be controlled.

For the sake of clarity, the logic behind the Steer – Steer Safety Maneuver will be explained based on the scenario shown in Figure 3.2, where the vehicles are driving at constant speed at 90° of each other. The proposed safety maneuver can be generalized for different intersections angles φ ϵ] 0°, 180° [.

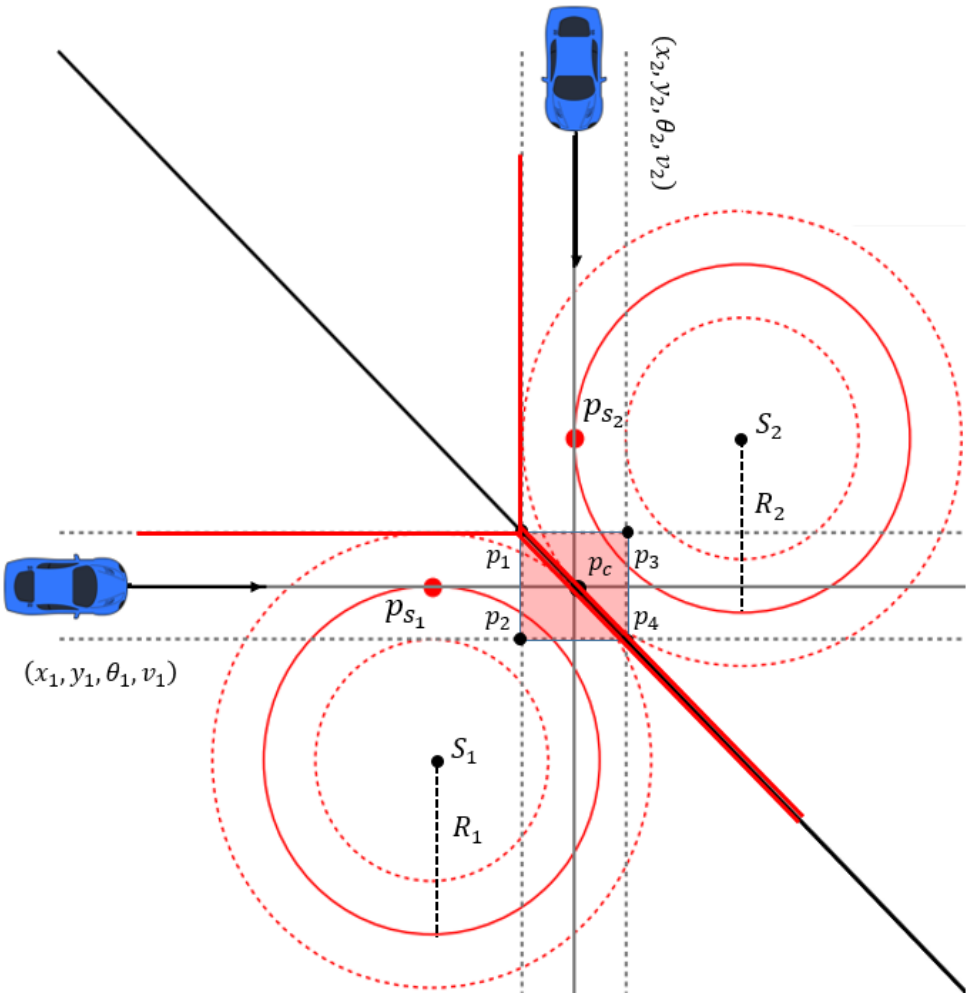

Figure 3.2: *Geometrical approach for Evasive Steering Maneuver.*

We start by defining the safety maneuver space as presented in Figure 3.2, which guarantees to get the vehicles as close as possible to the collision centre "p_c", in turn ensuring the latest activation of the safety maneuver at the last point to steer "p_{s_i}". For vehicle 1, the evasive maneuver is constrained by the vehicle's upper safe margin and a line dividing the collision area into two equal surfaces. For the configuration illustrated in Figure 3.2, this separation line passes through the points p_1, p_c and p_4.

In order to determine the last point to steer "p_{s_i}", point mass assumptions are used to describe the vehicle's motion. As speed is presumed to be constant, uniform circular motion equations are used to determine the steering radius, based on the forward speed v_i and a desired lateral acceleration a_{lat}, as follows:

$$R_i = \frac{v_i^2}{a_{lat}} \qquad \forall\, i \in \{1,2\} \tag{3.1}$$

From (3.1), the inverse relationship between the steering radius R_i and the lateral acceleration a_{lat} is evident. In other words, choosing a_{lat} as the maximum lateral acceleration that the vehicle can achieve leads to the smallest feasible steering radius, which in turn allows to get as close as possible to the collision area. For the analysis described in this thesis, we assume that the maximum lateral acceleration the vehicle can achieve is 1 g, where "g" is the acceleration due to the gravity. This lateral acceleration has been proven to be feasible from experiments conducted with passenger cars by Volvo Cars.

$$a_{lat} = 1\ g = 9.81 m/s^2 \tag{3.2}$$

Now that the safety maneuver space is defined, as well as the steering radius, the last point to steer is the only parameter left to be found. In Figure 3.3 it can be noted that a polygon is defined by the steering maneuver center "S_i", the tangent point to the upper safe margin $p_{T_{i_1}}$, the first corner of the collision area p_1, and the tangent point to the separation line $p_{T_{i_2}}$. This quadrilateral has two pairs of equal length sides, and each pair of opposing angles are supplementary angles. Based on the equations of the separation line and the upper safe margin, the angle β is calculated. Therefore, α is determined trivially as:

$$\alpha = 180° - \beta \tag{3.3}$$

In addition, we note that the line segment between $p_{T_{i_1}}$ and $p_{T_{i_2}}$ is a chord of the circle with radius $R_i + dR$, which defines the upper safe margin of the steering maneuver. The length of the chord is calculated with expression (3.4).

$$chord = 2\,(R_i + dR)\sin(\alpha/2) \tag{3.4}$$

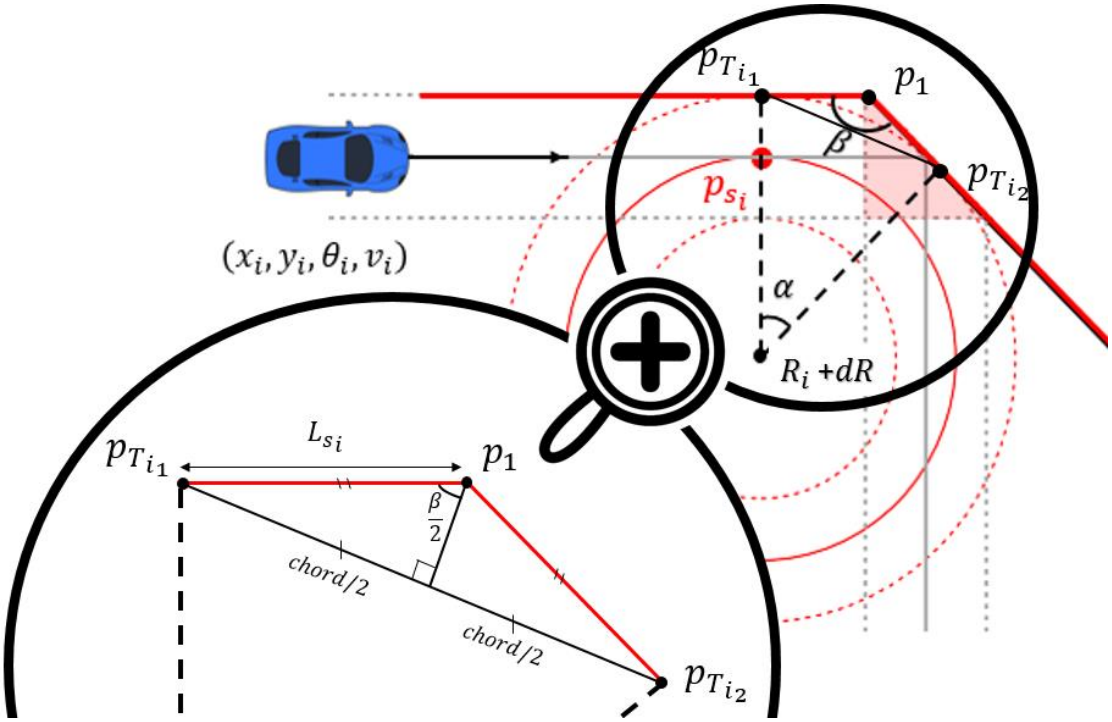

Figure 3.3: *Geometrical solution for Evasive Steering Maneuver.*

Therefore, the required steering distance " L_{s_i}" to avoid an overlap between the two vehicles is computed as:

$$L_{s_i} = \frac{chord/2}{\sin(\beta/2)} \tag{3.5}$$

By translating the point "p_1" along the upper safe margin by a distance "L_{s_i}" and performing an orthogonal projection onto the vehicle's path, the last point to steer "p_{s_i}" is determined, see Figure 3.3.

After finding the last point to steer "p_{s_i}", we divide the safe path into three portions with different driving actions: straight driving, steering, and braking, see Figure 3.4.

Consequently, collision-free trajectories can be generated ensuring the safe execution of the test case. More details about trajectory generation are discussed in section 3.4.

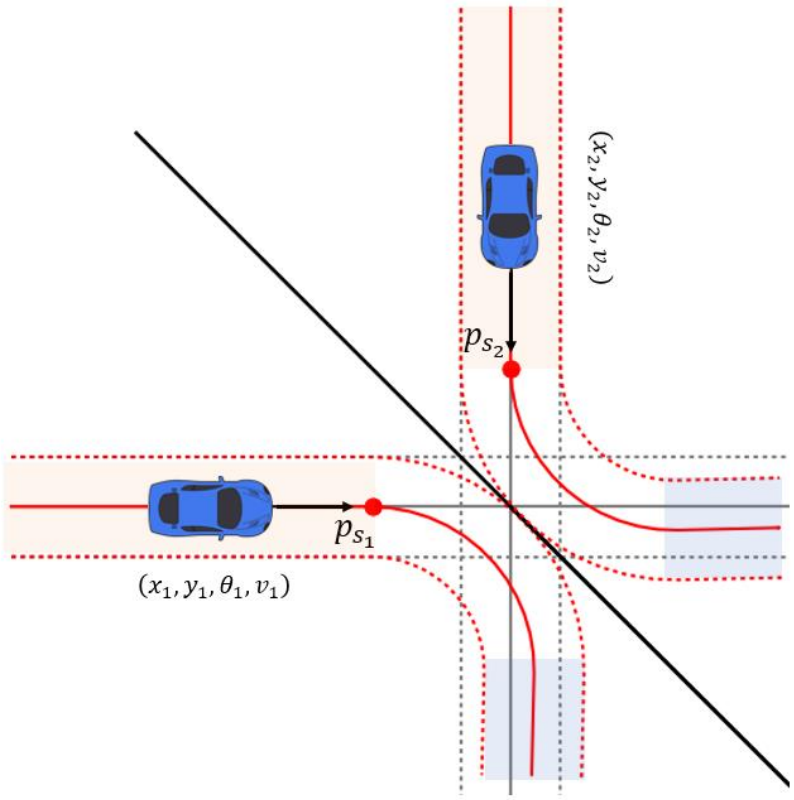

Figure 3.4: *Steer - Steer Safety Maneuver.*
Vehicles drive straight in the orange zone, steer with constant speed and constant lateral acceleration in the white zone, and brake in the blue zone.

3.1.3 Limitations

The capabilities of the vehicle and the driving robot should be taken into consideration in order to arrive at feasible manuevers. In (3.2) we assumed that the vehicle can achieve a maximum lateral acceleration of $1g$. This assumption is evaluated by performing several experiments discussed in Chapter 5.

The feasibility of the calculated steering radius, as defined in (3.1), for low driving speeds requires further analysis. We believe that the steering maneuver described before might be infeasible for low driving speeds. For low speeds, the steering radius required to develop a lateral acceleration of $1g$ becomes extremely small, even smaller than a car's length. As a result, the required steering angle exceeds the physical limit imposed by the vehicle and the driving robot. The experiments discussed in Chapter 5 provide further insight on the feasibility of the steering maneuver at low speeds. In the remainder of this thesis, we only analyse maneuvers above 20kph.

A different approach based on maximum steering angle instead of maximum lateral acceleration could be investigated for low speed scenarios. In the upcoming sections of this report, the Steer – Steer safety maneuver is not considered for scenarios with low speed. Instead, other safety maneuvers are analysed, such as Brake – Brake safety maneuver and Steer – Brake safety maneuver.

3.2 Brake – Brake Safety Maneuver

Similar to steering in [6], braking has been used for rear-end collision avoidance by decelerating during a required stopping distance "L_b", see Figure 3.5. "L_b" defines the last point to brake "p_b" behind the grey car where the blue car must start braking at least to avoid collision.

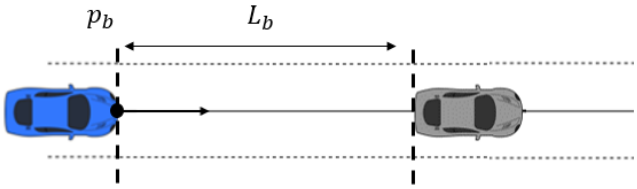

Figure 3.5: *Illustration of autonomous rear-end collision avoidance [6] by applying a braking action.*
The blue car represents the controllable object and in contrast the grey car represents the obstacle.

3.2.1 Approach

Following analogous steps as for the Steer – Steer Safety Maneuver, we have started by defining the safety maneuver space. It must guarantee to get the vehicles as close as possible to the collision centre in turn providing the latest activation of the safety maneuver at the last point to brake " p_{b_i}", see Figure 3.6.

The evasive braking maneuver is delimited by making the front bumper of the vehicles stop at the stop point "p_{st_i}", see Figure 3.6. The stop point "p_{st_i}" is calculated through an orthogonal projection of "p_1" onto the estimated paths to ensure that the vehicles will not enter the collision area.

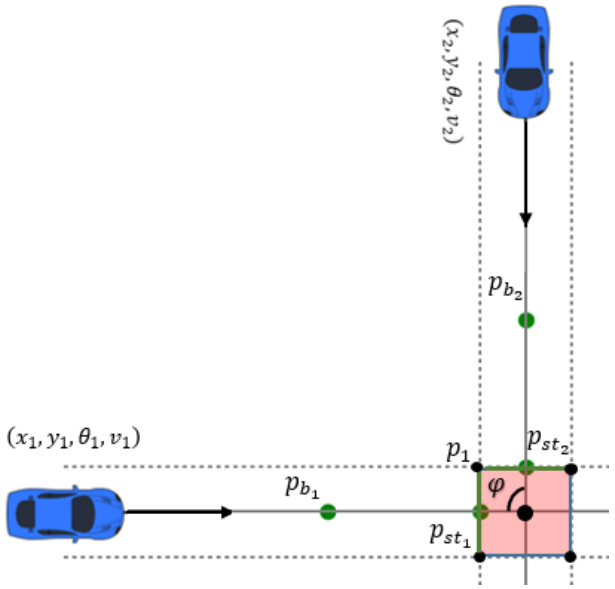

Figure 3.6: *Geometrical approach for Evasive Braking Maneuver* $\varphi = 90°$.

Notice that, for intersection angles below 90°, this orthogonal projection gives a conservative stopping point, see Figure 3.7. On the other hand, for intersection angles above 90°, the orthogonal projection leads to a stopping point quite dangerous, especially for high speeds where the inertia might not make the vehicles respect the stop point, see Figure 3.8. The bigger the intersection angle, the more dangerous the situation becomes. To overcome this safety issue for intersection angles above 90°, we propose to perform an orthogonal projection for one vehicle and a translation operation for the other to calculate the corresponding safe stop points as shown in figure 3.8.

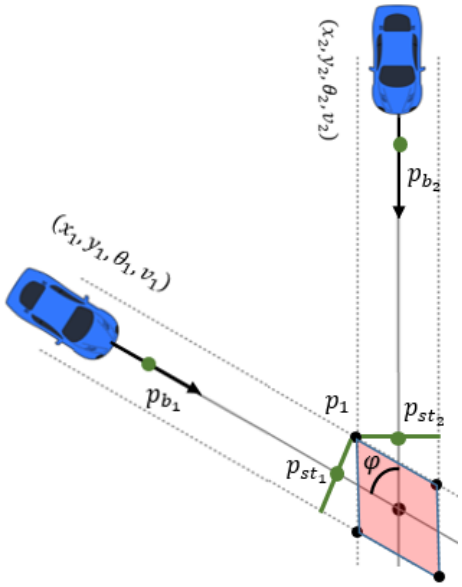

Figure 3.7: *Geometrical approach for Evasive Braking Maneuver* $\varphi = 30°$.

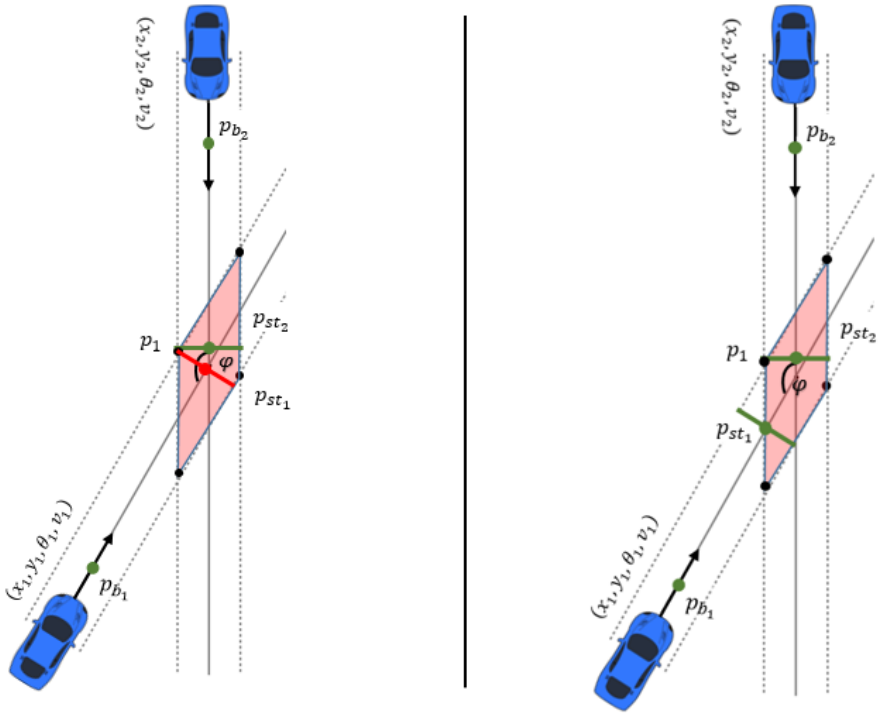

Figure 3.8: *Geometrical approach for Evasive Braking Maneuver* $\varphi = 150°$.
On the left: Dangerous Approach. On the right: Safe Approach.

Furthermore, by assuming point mass equations of motion and that the maximum achievable longitudinal deceleration "a_{dec}" is $0.8g$ (3.6), the required braking distance "L_{b_i}" can be found. This deceleration has been proven to be feasible from experiments conducted with passenger cars by Volvo Cars.

$$a_{dec} = -0.8g = -7.848\, m/s^2 \tag{3.6}$$

For vehicle i represented in Figure 3.9, the longitudinal distance travelled in time "t" is:

$$L_t = v_{i_0} t + \frac{1}{2} a_{dec} t^2, \text{ where } v_{i_0} \text{ is the initial velocity} \quad \forall\, i \in \{1,2\} \tag{3.7}$$

And the velocity varies over a time "t" according to:

$$v_{i_t} = v_{i_0} + a_{dec} t \qquad \forall\, i \in \{1,2\} \tag{3.8}$$

Equating (3.8) to zero, the time needed to stop the vehicle corresponds to:

$$t_{st} = -\frac{v_{i_0}}{a_{dec}} \qquad \forall\, i \in \{1,2\} \tag{3.9}$$

By substituting (3.9) in (3.7), the braking distance "L_{b_i}" is:

$$L_{b_i} = -\frac{1}{2} v_{i_0}^2 / a_{dec} \quad \forall\, i \in \{1,2\} \tag{3.10}$$

Finally, by translating "p_{st_i}" a distance "L_{b_i}" along the vehicle's estimated path, the last point to brake "p_{b_i}" is defined, see Figure 3.9.

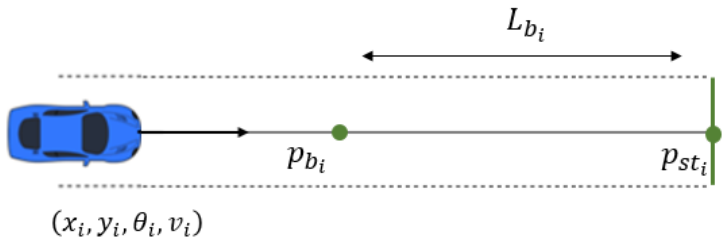

Figure 3.9: *Geometrical solution for Evasive Braking Maneuver.*

Based on the last point to brake "p_{b_i}", we divide the safe path into two portions with two different driving actions: straight driving and braking, see Figure 3.10. Consequently, collision-free trajectories can be generated ensuring the safe execution of the test case. More details about trajectory generation are given in section 3.4.

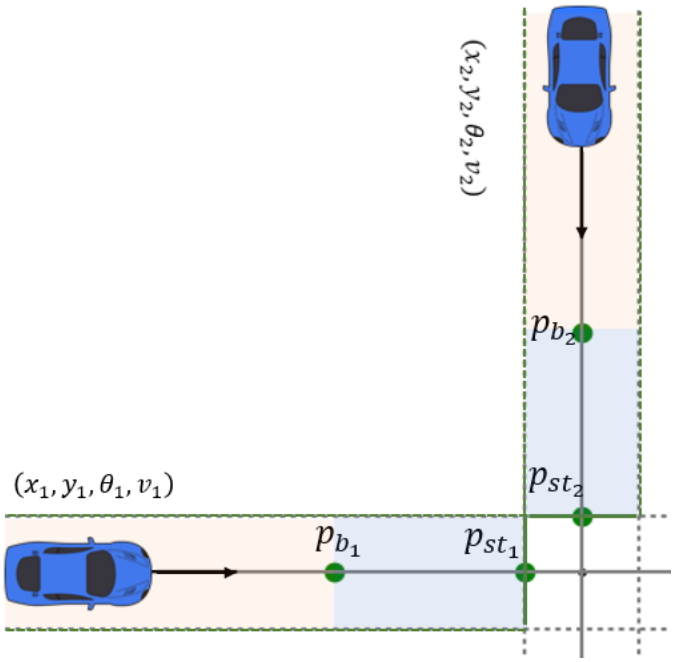

Figure 3.10: *Brake – Brake Safety Maneuver.*
Vehicles drive straight in the orange zone, and brake in the blue zone.

3.3 Steer – Brake Safety Maneuver

Combining steering and braking in a safety maneuver has the potential to optimize the position of the last point to react. We have started by defining which vehicle will apply which emergency action. The lower the speed of the vehicle, the shorter the braking distance is, a direct relation that can be verified by (3.10). In the following explanation, the slower vehicle is denoted with the index "$i = 2$". This vehicle will brake and come to a stop at "p_{st_2}" located on the far edge of the collision area as shown in Figure 3.11. The rational discussed in section 3.2 is applied to determine the last point to brake for vehicle "$i = 2$". For vehicle "$i = 1$", we compare two steering alternatives illustrated in Figure 3.11. The alternative that minimizes the distance between the last point to steer "p_{s_1}" and the collision center "p_c" is selected.

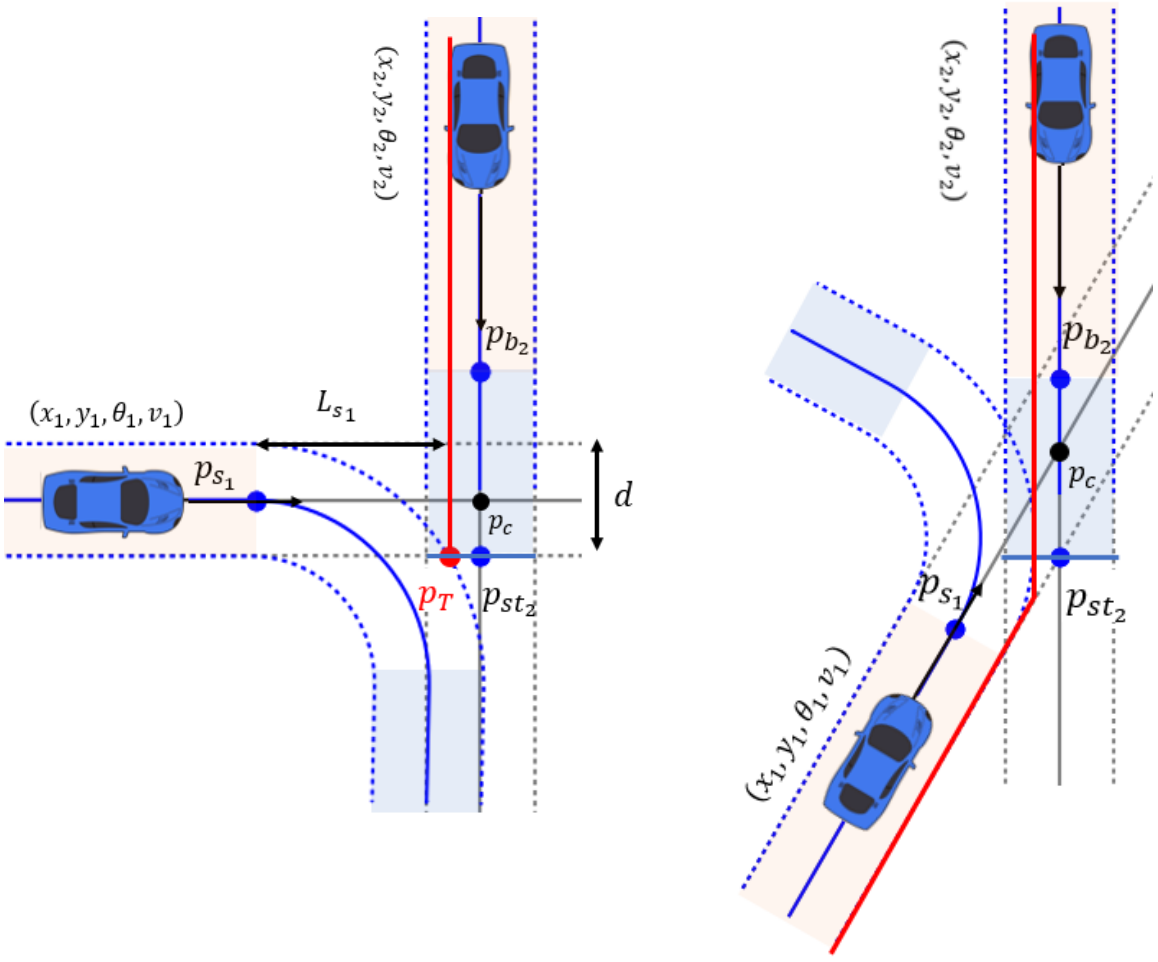

Figure 3.11: *Steer – Brake Safety Maneuver.*
Clockwise Steering (left) and Counter-Clockwise Steering (right)
Vehicles drive straight in the orange zone, steer with constant speed in the white zone, and brake in the blue zone

3.3.1 Clockwise Steering Approach

It is inspired from the rear-end collision avoidance maneuver [6] presented in section 3.1.1. It is based on achieving a certain lateral displacement "d" at a predefined specific point in order to avoid overlapping.

The required lateral displacement in our approach is the width of the collision area "d", which is the distance between the two safe margins of the vehicle. This lateral displacement must be attained at point "p_T" as represented in Figure 3.11 in order to avoid collision. We could have used a corner of the collision area instead of "p_T", but it would be conservative since it is still safe to achieve the lateral displacement at point "p_T".

As discussed in section 3.1, the motion of the vehicle while steering is assumed to be described by point mass equations of motion as well as to keep constant speed along the path. Therefore, for vehicle "$i = 1$" in Figure 3.11, the required steering radius is calculated based on (3.1) and (3.2).

The longitudinal displacement "L" over a time "t" is determined according to:

$$L_t = v_i t \qquad \forall\, i \in \{1,2\} \tag{3.11}$$

The lateral displacement over a time "t" is given by:

$$d_t = \frac{1}{2} a_y t^2 \tag{3.12}$$

By eliminating time from (3.11) and (3.12) and setting $d_t = d$, the required steering distance is:

$$L_{s_1} = v_i \sqrt{2d/a_y} \qquad \forall\, i \in \{1,2\} \tag{3.13}$$

As a result, the last point to steer "p_{s_1}" is found by translating "p_T" on the lower safe margin a distance "L_{s_1}" and performing an orthogonal projection onto the vehicle's estimated path.

3.3.2 Counter-Clockwise Steering Approach

It is inspired from the Steer – Steer Safety Maneuver approach and has the same geometrical solution. We have just defined the steering space differently as shown in Figure 3.11 in order to be the least conservative yet safe. A detailed explanation on how to find the last point to steer "p_{s_1}" was given in section 3.1.2.

3.3.3 Limitations

The proposed Steer – Brake Safety Maneuver is not optimal neither safe for intersection angles below 90°. Concerning the clockwise steering approach, the desired lateral displacement for vehicle "$i = 1$" is attained at the desired point "p_T". However, while conducting the steering maneuver the path of vehicle "$i = 1$" overlaps with that of vehicle "$i = 2$", as illustrated in Figure 3.12.

On the other hand, for the counter-clockwise approach, in order to respect the boundaries of the steering maneuver space, the last point to steer "p_{s_1}" is very far from the collision center. Therefore, for safety requirements and computational efficiency, the Steer – Brake Safety Maneuver is discarded for intersection angles below 90°.

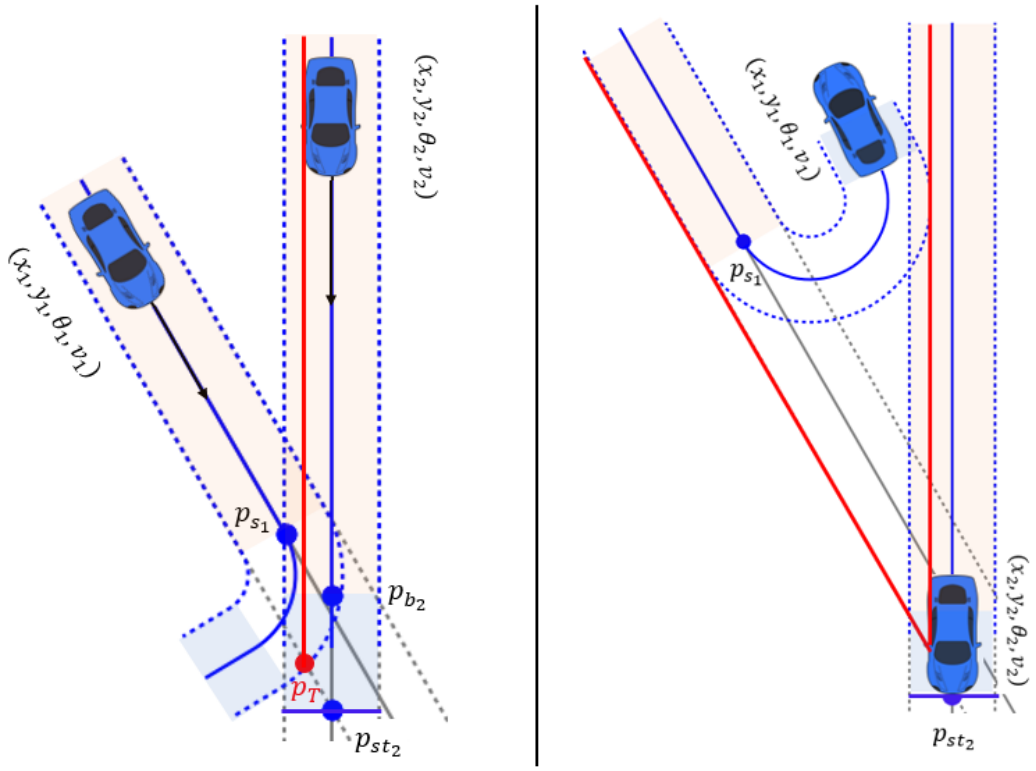

Figure 3.12: *Steer – Brake Safety Maneuver.*
Clockwise Steering (left) and Counter-Clockwise Steering (right)
Vehicles drive straight in the orange zone, steer with constant speed in the white zone, and brake in the blue zone

3.4 Maneuver-Based trajectory generation

In this section, we explain how the collision-free trajectories are generated in order to finalize the development of the supervisor module. The supervisor, in case of collision detection, generates safe trajectories and send them to the driving robots. The path following controller of the driving robot requires a set of nodes along the desired trajectory or path to be followed in order to calculate the adequate steering angle, speed, and accelerations. Therefore, the collision-free trajectories commanded to the driving

robot are discretized and each node " k" of the trajectory contains the following information:

- i: vehicle index $i \in \{1,2\}$
- t_k: time stamp $t_k \in \mathbb{R}^+$, with $k \in \mathbb{N}$
- $(x_{i_k}, y_{i_k}, \theta_{i_k}, v_{i_k})$: states of vehicle i at time t_k

In the previous sections, we explained and detailed how the safety maneuvers were developed seeking to position the last point to react as close as possible to the collision area. Since point mass equations are used to describe the vehicle's motion, vehicles' states along the safe path are easily generated. The evasive maneuver path is divided into various portions according to the undertaken driving action and each portion of the path is calculated under some assumptions invoked further.

For simplicity, we will only demonstrate the trajectory generation for one vehicle "i" with an initial heading angle "$\theta_{i_0} = 0°$" as presented in Figure 3.13, and Figure 3.14.

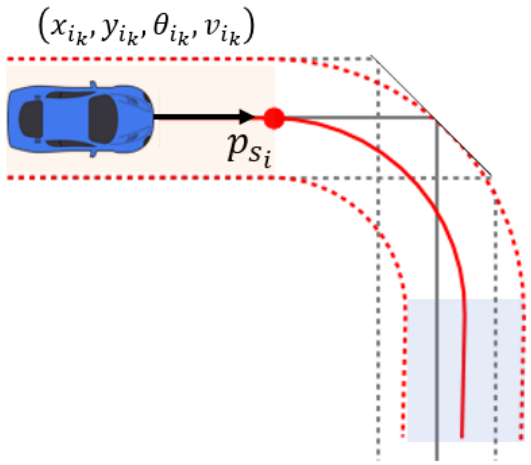

Figure 3.13: *Trajectory generation for a Steering Maneuver.*
Vehicles drive straight in the orange zone, steer with constant speed in the white zone, and brake in the blue zone.

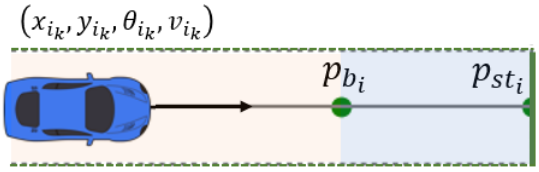

Figure 3.14: *Trajectory generation for a Braking Maneuver.*
Vehicles drive straight in the orange zone, and brake in the blue zone.

- **Drive Straight nodes:** $\boldsymbol{a_{dec} = 0 \; and \; a_{lat} = 0}$

The collision-free trajectories also serve as back-up trajectories in case of loss of communication. That is why we add this portion of trajectory to guarantee a safe exit under any circumstance. In case of loss of communication, we want the vehicles to

continue driving straight until reaching the last point to react, instead of triggering the safety maneuver as soon as communication is lost. Therefore, while vehicle i has not yet reached the last point to react "p_{s_i} *or* p_{b_i}", the trajectory nodes are calculated as follows:

$$x_{i_k} = x_{i_0} + v_{i_0} t_k \qquad \forall\, i \in \{1,2\}\ and\ k \in \mathbb{N} \tag{3.14}$$

$$y_{i_k} = y_{i_0} \qquad \forall\, i \in \{1,2\}\ and\ k \in \mathbb{N} \tag{3.15}$$

$$v_{i_k} = v_{i_0} \qquad \forall\, i \in \{1,2\}\ and\ k \in \mathbb{N} \tag{3.16}$$

$$\theta_{i_k} = \theta_{i_0} \qquad \forall\, i \in \{1,2\}\ and\ k \in \mathbb{N} \tag{3.17}$$

- **Steering nodes: $a_{dec} = 0$ *and* $a_{lat} = 1g$**

In this maneuver, we assume that the forward velocity remains constant along the path:

$$v_{i_k} = v_{i_0} \qquad \forall\, i \in \{1,2\}\ and\ k \in \mathbb{N} \tag{3.18}$$

The angular velocity " ω ", which is also assumed to be constant during the steering maneuver, is used to determine the end of the steering portion and to update the heading angle state.

The angular velocity is determined as follows:

$$\omega = \frac{v_{i_0}}{R_i} \tag{3.19}$$

The criterion to end the steering section of the maneuver is set: $\Delta\theta = 90°$. That is to ensure a sufficient displacement avoiding overlapping for any collision angle studied in this thesis work. Therefore, while $\Delta\theta \leq 90°$, the heading of the vehicle is updated as follows:

$$\theta_{i_k} = \theta_{i_0} \pm \omega\, \Delta t \qquad \forall\, i \in \{1,2\}\ and\ k \in \mathbb{N} \tag{3.20}$$

Note that in (3.20), the "$\pm$" operation accounts for the steering direction; "$+$" for counter-clockwise steering and "$-$" for clockwise steering.

A rotating frame (γ, μ) is seen to simplify the description of the vehicle's motion during the steering maneuver. At every sampling time "t_s", the fixed reference frame(x, y) is rotated "θ_{i_k}" to obtain the rotating frame corresponding to the time stamp "t_k". The rotation is done around the z axis as illustrated in Figure 3.15.

Every sampling time "t_s", the forward speed "v_{i_0}" is assumed constant in $\vec{\gamma}$, and the lateral acceleration "a_{lat}" is assumed constant in $\vec{\mu}$. Therefore, the displacement of the vehicle in the rotating frame is expressed as:

$$\gamma = v_{i_0} t_s \tag{3.21}$$

$$\mu = \frac{1}{2} a_{lat} t_s^2 \tag{3.22}$$

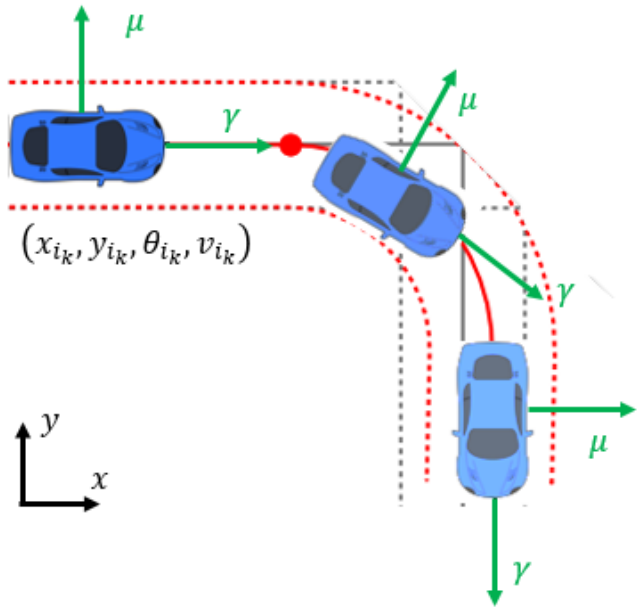

***Figure 3.15**: Illustration of relating a moving frame to fixed reference frame*

Finally, the transformation from rotating coordinates (γ, μ) to fixed coordinates (x, y) can be written:

$$x_{i_k} = x_{i_{k-1}} + \gamma \cos(\theta_{i_k}) + \mu \sin(\theta_{i_k}) \qquad \forall\, i \in \{1,2\} \text{ and } k \in \mathbb{N} \tag{3.23}$$

$$y_{i_k} = y_{i_{k-1}} + \gamma \sin(\theta_{i_k}) - \mu \cos(\theta_{i_k}) \qquad \forall\, i \in \{1,2\} \text{ and } k \in \mathbb{N} \tag{3.24}$$

- **Braking nodes: $a_{dec} = -0.8g$ and $a_{lat} = 0$**

The braking maneuver reaches an end when the vehicle totally stops. Consequently, while $v_{i_k} > 0$, the trajectory nodes are calculated as follows:

$$x_{i_k} = x_{i_0} + (v_{i_0} t_k + \frac{1}{2} a_{dec} t_k^2) \cos(\theta_{i_k}) \qquad \forall\, i \in \{1,2\} \text{ and } k \in \mathbb{N} \tag{3.25}$$

$$y_{i_k} = y_{i_0} + (v_{i_0} t_k + \frac{1}{2} a_{dec} t_k^2) \sin(\theta_{i_k}) \qquad \forall\, i \in \{1,2\} \text{ and } k \in \mathbb{N} \tag{3.26}$$

$$v_{i_k} = v_{i_0} + a_{dec} t_k \qquad \forall\, i \in \{1,2\} \text{ and } k \in \mathbb{N} \tag{3.27}$$

$$\theta_{i_k} = \theta_{i_{k-1}} \qquad \forall\, i \in \{1,2\} \text{ and } k \in \mathbb{N} \tag{3.28}$$

3.5 Evaluation

In this section, we will discuss the performance of the proposed safety maneuvers based on the time to collision (TTC) criterion. The time to collision outlines how far the vehicles are from the collision center at the activation of the collision-free trajectories. To put it differently, it represents the time the vehicle would take to reach the collision center starting from the last point to react, assuming that the vehicle would have kept constant speed and constant heading instead of applying the safety maneuver.

In some cases, the time to collision (TTC) for one vehicle is different from the other vehicle due to different speeds or initial positions. Therefore, we only consider the larger time to collision (TTC) as it reflects the triggering time of the whole safety maneuver.

For the current vehicle in the loop (VIL) test framework, it is important to point out that we will not be able to test speeds above 60 kph due to space limitations on the test track. To be able to compare theoretical results and experimental results, we examined the time to collision (TTC) attained with our safety maneuvers for speeds between 5 m/s and 17 m/s, which is also the range of speeds used for the experiments discussed in Chapter 5.

Data were collected by analyzing angled collision scenarios for several intersection angles between 10° and 170° with several speed combinations within the previuosly-mentioned speed range. Vehicles initial positions were 30s behind the collision center and for each scenario we calculated the last point to react in order to derive the time to collision (TTC).

We analysed the data by plotting heat maps. The heat map illustrates, for every speed combination, how close the vehicles are from the collision center at the activation of the safety maneuver. It is evident by comparing the range of time to collison (TTC) in figures 3.14, 3.15 and 3.17 that the Brake – Brake Safety Maneuver has larger time to collision (TTC) than the Steer – Steer Safety Maneuver and the Steer – Brake Safety Maneuver. This finding implies that, for the scenarios considered in these figures, the last point to brake is farther away from the collision center compared to the last point to steer.

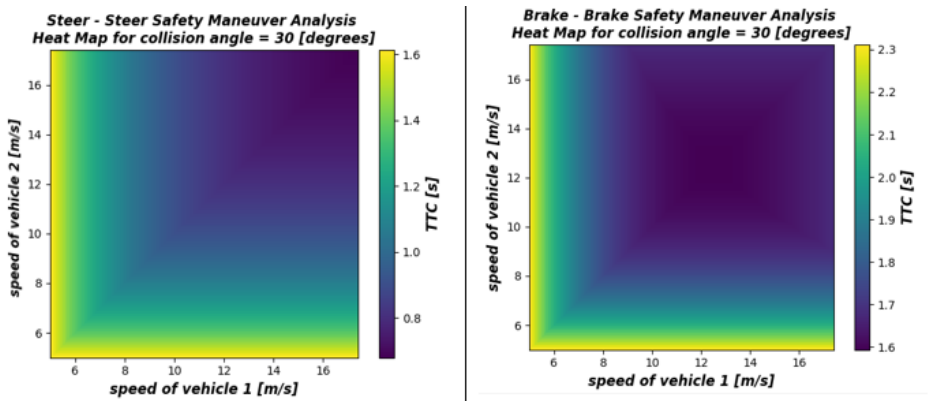

Figure 3.16: *Heat Maps for collision angle* $\varphi = 30°$.

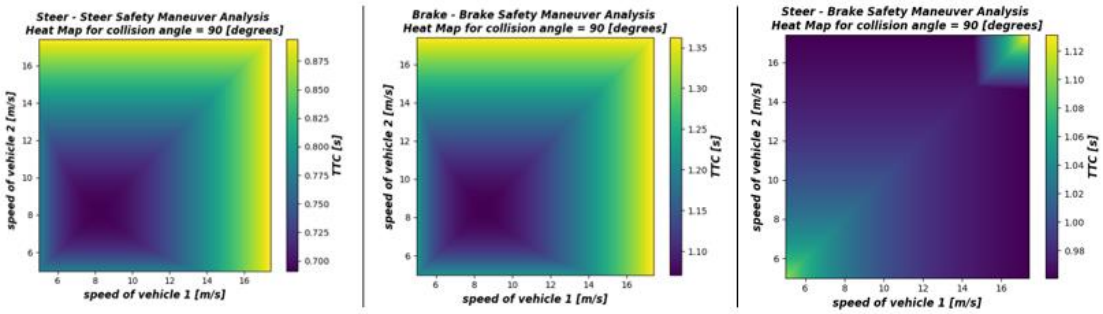

Figure 3.17: *Heat Maps for collision angle* $\varphi = 90°$.

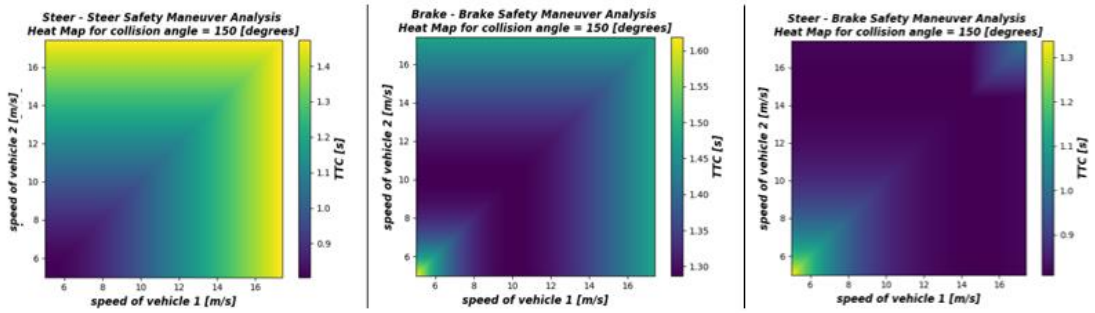

Figure 3.18: *Heat Maps for collision angle* $\varphi = 150°$

For the interested readers, a comparison between the three safety maneuvers for each intersection angle φ ϵ] 0°, 180° [via heat maps is given in Appendix I.

Heat maps represent an excellent tool to evaluate the performance of a specific maneuver at a specific collision angle. Therefore, test engineers can easily choose which scenarios are adequate to validate the desired functions. To put it differently, in order to test a function, the vehicles should reach its activation time, consequently the last point to react should be positioned after the activation time of the tested function. However, heat maps do not give a global overview on the performance of the safety maneuver.

As a result, we decided to calculate the average time to collision (TTC) of each heat map. Plotting the average TTC as a function of collision angle, as shown in Figure 3.19, allows to elicit further data that provides a better perspective. The reason for considering the Steer – Brake Maneuver for intersection angles only above 90° is discussed in section 3.3.3. The data illustrates the superiority of the Steer – Steer Safety Maneuver for collision angles below 120° and of the Steer – Brake Safety Maneuver for collision angles above 120°. It also casts a light on the performance of the Brake – Brake Safety Maneuver and eliminate it from the competition with the other safety maneuvers.

Nevertheless, the supervisor will be comparing the three maneuvers constantly in order to select the optimal maneuver, as discussed in Chapter 4. Therefore, we expect that the supervisor will behave as illustrated in Figure 3.19. Our findings are very promising since for collision angles between 30° and 160°, we see that the supervisor will abort the test and activate the optimal safety maneuver at most 1s before any collision occur.

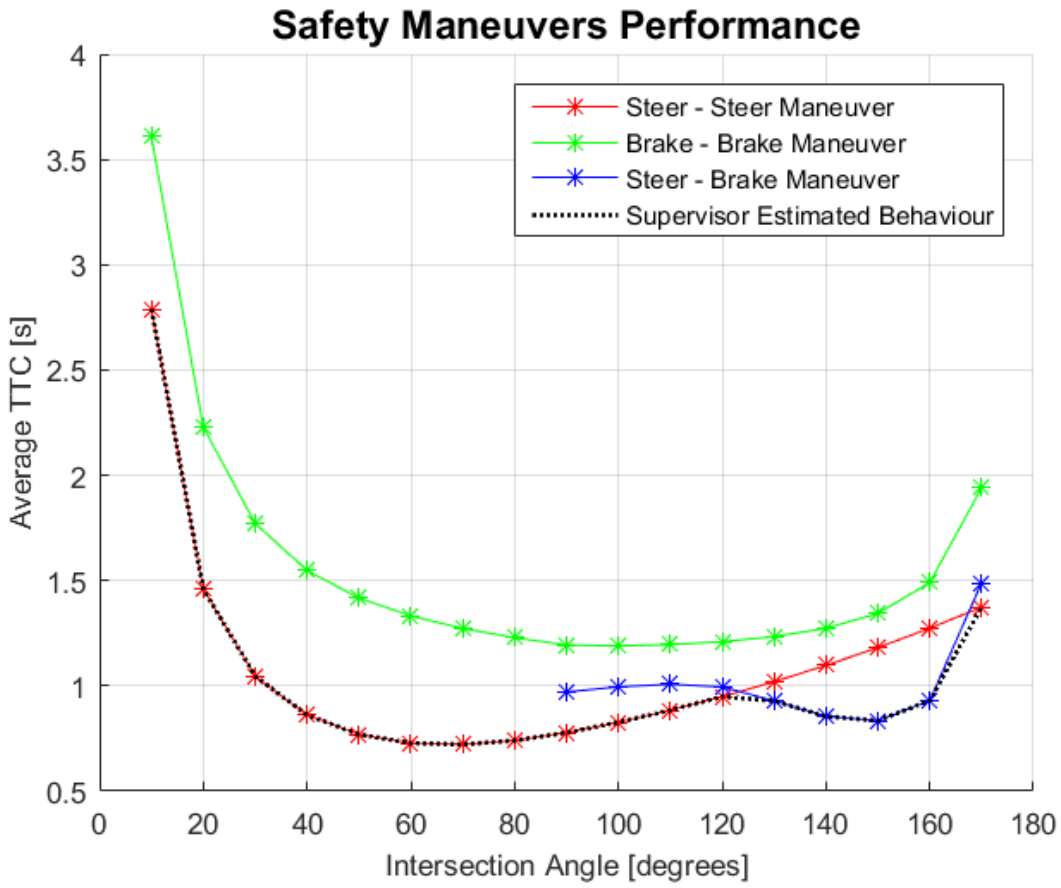

Figure 3.19: *Safety Maneuvers' Perfomance.*
The red, green, and blue curves illustrate the average time to collision (TTC) achieved with the developed safety maneuvers for scenarios with different intersection angles. The average TTC is computed from the TTCs obtained for scenarios with a specific intersection angle but with various combinations of driving speeds. TTC refers to the time it would take the vehicles to reach the collison center from the last point to react if the vehicles would have kept constant speed. The dashed curve represents the predicted performance of the supervisor module in aborting the test case by choosing the optimal safety maneuver to apply among the three proposed maneuvers.

4 Implementation Of The Supervisor Module

In this Chapter, we describe the functional architecture of the supervisor module and define its performance based on a benchmark set by the results presented at the end of this chapter.

4.1 Functional Architecture

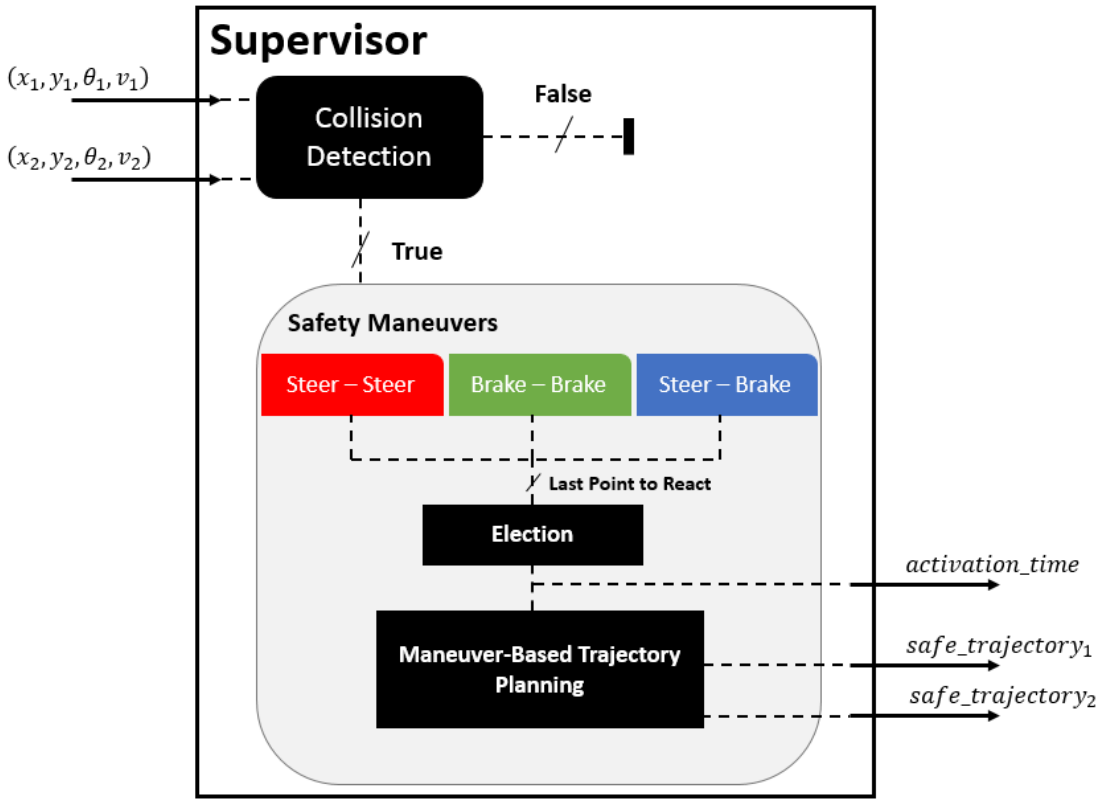

Figure 4.1: *Supervisor Functional Architecture.*

The functional architecture of the supervisor module is illustrated in Figure 4.1. The supervisor takes as inputs the vehicles' current states and gives as outputs the safe trajectories and an activation time which stands for the last point to react of the selected maneuver.

The collision detection module was developed according to the strategy described in Chapter 2. If the output of this module is "False", the test is considered safe. No emergency action is required since no collision was detected. Otherwise, safety maneuvers' analysis are launched in order to calculate the last point to react as we have seen in chapter 3. The election function simply compares the last point to react of the safety maneuvers in order to define the optimal evasive maneuver. This comparison is done by analysing the time to collision (TTC), which is the time elapsed between the last point to react and the collision center if the vehicles would keep constant speed and constant heading. The

safety maneuver with the minimum time to collision (TTC) is considered optimal and its safe trajectories are generated and sent to the test vehicles. It must be pointed out that collision-free trajectories are also back-up trajectories. They are only activated either at the last point to react or immediately in case of loss of communication.

4.2 Evaluation

In section 3.5, we have estimated the behaviour of the supervisor based on the optimal safety maneuver behaviour at each collision angle. It is important to note that the performance of the maneuver is measured via the average time-to-collision (TTC) achieved for a particular collision angle. It reflects how far the vehicles are from the collision center at the activation of the safe trajectories.

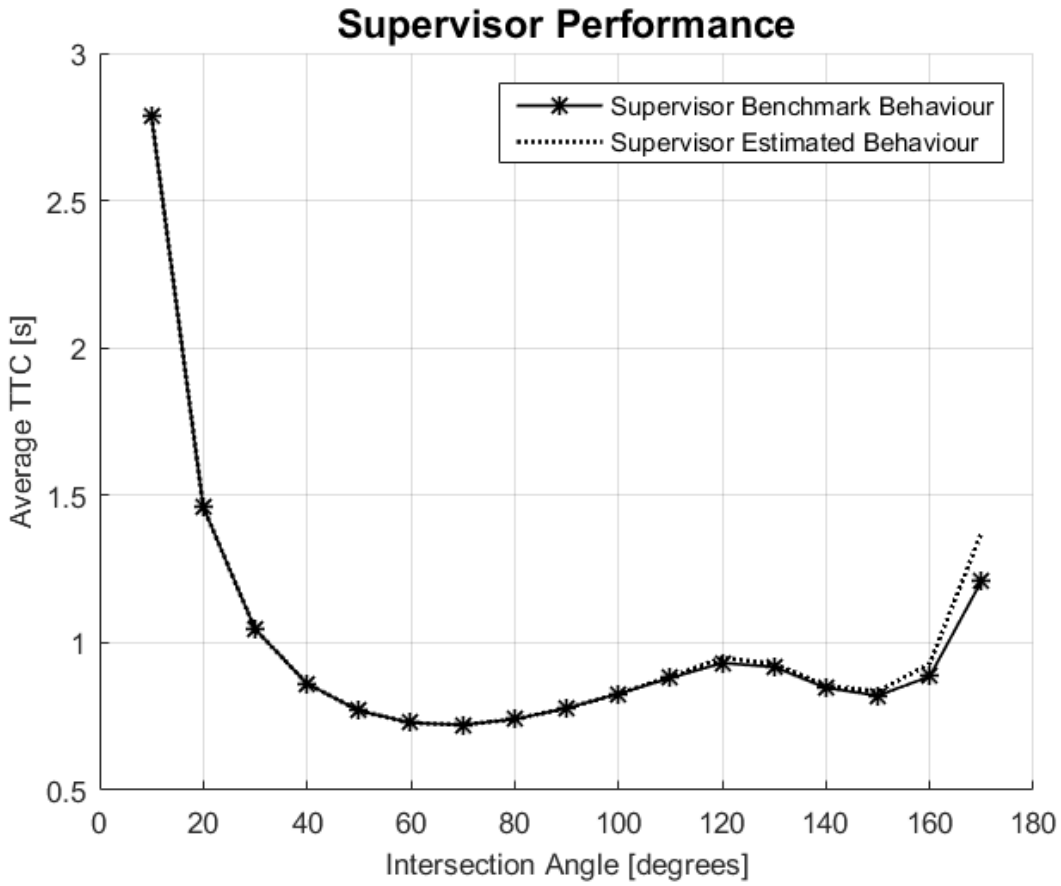

Figure 4.2: *Supervisor Performance.*
The black solid curve illustrates the performance of the supervisor module in aborting the test case by applying the optimal safety maneuver. The dashed curve represents the predicted behaviour of the supervisor module. The average TTC is computed from the TTCs obtained for scenarios with a specific intersection angle but with various combinations of driving speeds. TTC refers to the time it would take the vehicles to reach the collison center from the last point to react if the vehicles would have kept constant speed.

After implementing the supervisor module, we ran the exact same scenarios defined in section 3.5 in order to verify our prior analysis and define a benchmark of the supervisor's performance, see Figure 4.2.

Planned comparisons revealed that the supervisor as expected switch between Steer-Steer Safety Maneuver and Steer-Brake Safety Maneuver at 120°. The benchmark perfectly follows the estimated behaviour until 110° then slightly goes down. This finding indicates good results, even if the improvement is modest.

To explain the improvement on performance illustrated in Figure 4.2, we generated heat maps as illustrated in figures 4.3, 4.4, 4.5. For collision angles above 100°, the optimal safety maneuver also depends on the speed of the vehicles and not only the intersection angle.

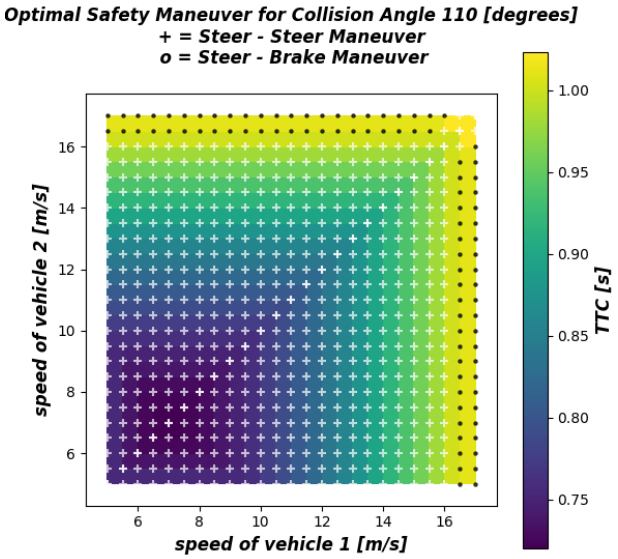

Figure 4.3: *Heat Maps for collision angle* $\varphi = 110°$.

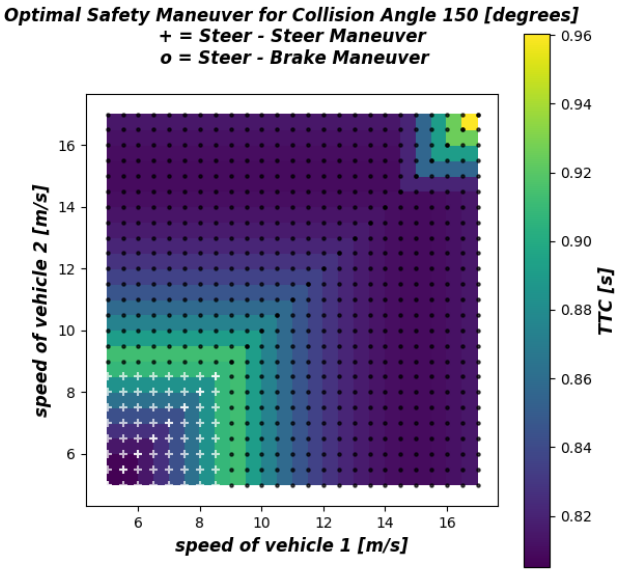

Figure 4.4: *Heat Maps for collision angle* $\varphi = 150°$.

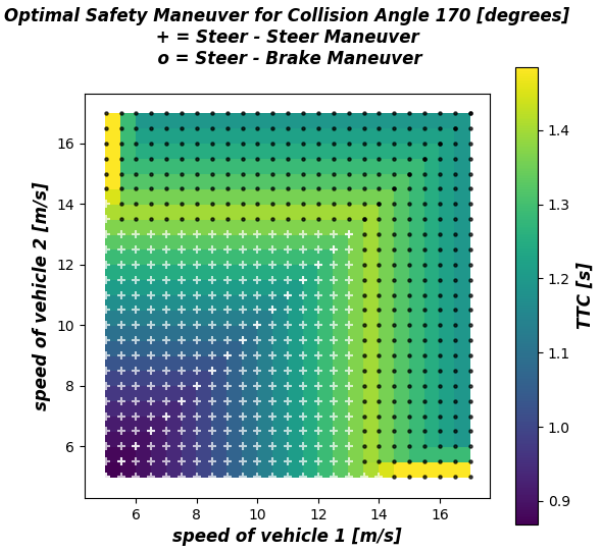

Figure 4.5: *Heat Maps for collision angle* $\varphi = 170°$.

For the interested readers, optimal safety maneuver heat maps for each collision angle $\varphi \in]\, 0°, 180° \,[$ are given in Appendix II.

5 Experimental Verification

Collision-free trajectories are generated by modelling the vehicle motion with kinematic point mass equations, assuming a maximum lateral acceleration of $1g$ (3.2) and a maximum deceleration of $0.8g$ (3.6). The feasibility of the trajectories delivered by the supervisor module was tested by performing a set of experiments. Maneuver-based trajectories comprised of braking and steering were generated and tested for a speed range between 20kph and 60kph. Our findings had been used to guarantee the drivability of the calculated trajectories by tuning the lateral acceleration value and adjusting the stop point for some braking maneuvers. Each test was performed twice with the same initial conditions to ensure the quality of the test and the accuracy of the collected data.

5.1 Test Environment

Volvo Cars supplied us with all equipment and technical support needed to perform the desired experiments. The test track area was 350m long and 120m large in its widest part which restricted the speed of the maneuvers to be between 20kph and 60kph. Data was logged by driving a Volvo XC90. Therefore, trajectories were generated based on the dimensions illustrated in Figure 5.1. The safe margin is defined based on the vehicle's width, see section 2.3. Latitude and longitude location in the trajectory's nodes had to be translated as the driving robot requires that the coordinates should be given based on the front wheel axle position.

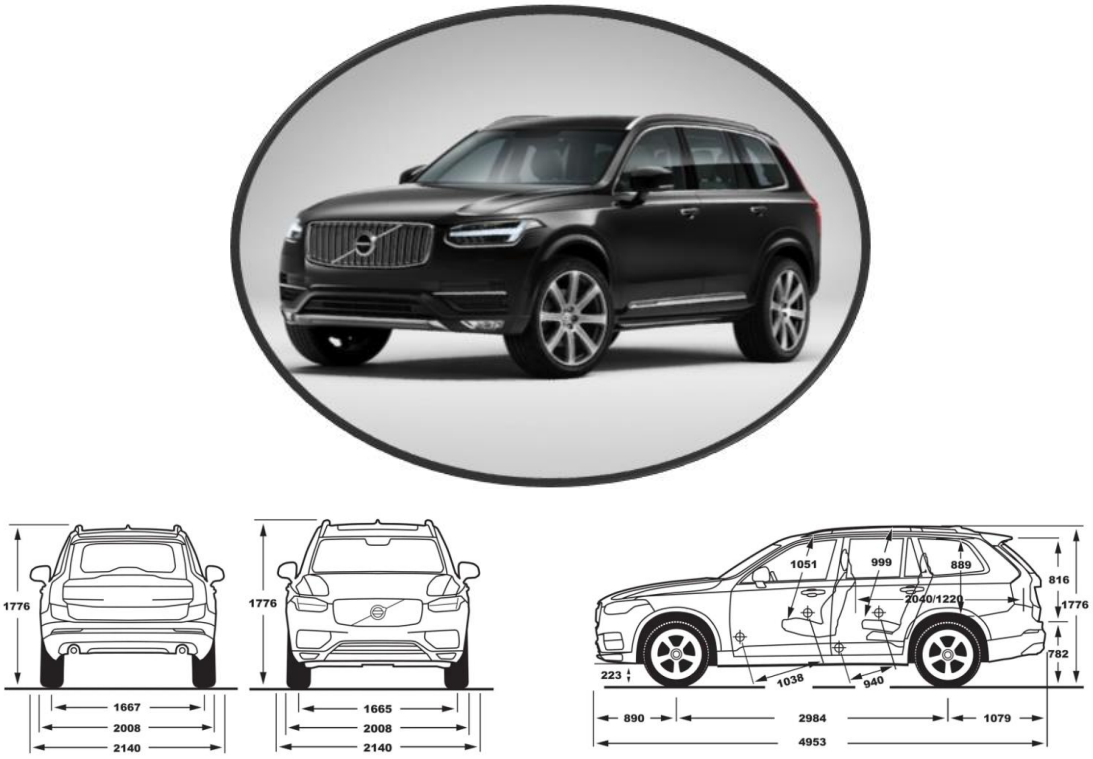

Figure 5.1: *XC90 Volvo Car 2019 (Source: Volvo Cars)*

The driving robot mounted in the vehicle includes two modules: steering module and braking module as shown in Figure 5.2. They collaborate together in order to take full control of the vehicle and follow any given path with an accuracy that no human driver can achieve thanks to the path following controller. A motion pack is equipped in order to track the vehicle's exact current position via GPS signals and an Inertial Measurement Unit. With measurements of the current position, velocity, and heading, the controller is able to generate the required control signals to apply the adequate force on the pedals and torque on the steering wheel to follow the desired path. A simplified control scheme is illustrated in Figure 5.3.

Figure 5.2: *Steering Robot on the left, and Pedals Robot on the right.*

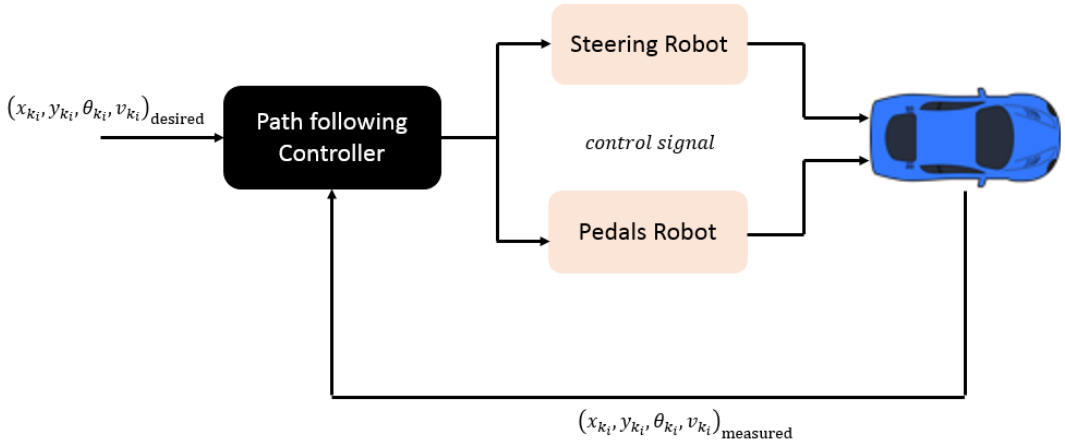

Figure 5.3: *Simplified Control Scheme of the path following controller*

The path following error will thus be evaluated by calculating the distance between the measured position and the desired position in the trajectory node with the timestamp that matches the measurement time, see Figure 5.4 for a visual explanation.

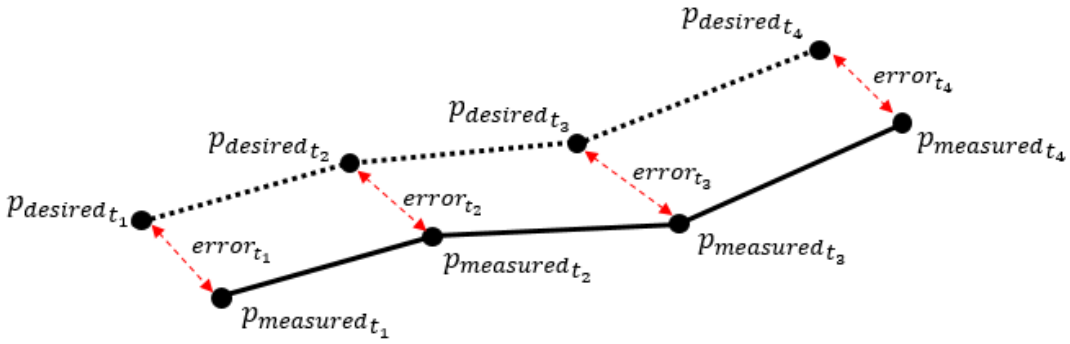

Figure 5.4: *Path Following Error Illustration*

5.2 Steering Maneuver Validation

Collision-free steering-based trajectories were generated for a speed range between 20kph and 60kph with an increment of 10kph. The trajectory is comprised of 3 portions: drive straight with constant speed until reaching the last point to steer. Steering to achieve a maximum lateral acceleration assumed to be $1g$. Once performing an angular displacement of 90°, braking is requested to stop the test, see Figure 5.5. Maneuver-based trajectory generation is explained in section 3.4. The validation of the steering maneuver is done by evaluating the path following controller performance. To put it differently, we verify if the path following error is below our safety margin considered to be 1m. Since kinematic point mass equations model the vehicle's motion, it is desired to verify if the generated trajectories are physically driveable.

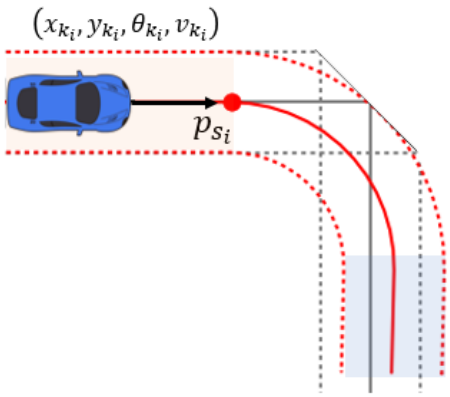

Figure 5.5: *Trajectory generation for a Steering Maneuver.*
Vehicles drive straight in the orange zone, steer with constant speed in the white zone, and brake in the blue zone.

The vehicle has successfully followed the given collision-free paths for speeds between 20kph and 50kph with a path following error less than 1m which is our safety margin. However, the car drifted and the test was aborted for tests conducted at 60kph. In Figure

5.6, we see how the path following error rapidly increases for 60kph due to the drifting phenomena.

The results demonstrate two things. First, the higher the velocity, the lower the steering wheel angle required to follow the prescribed trajectory. It is notable that at 20kph, the steering wheel angle is huge, almost -600°, see Figure 5.6. In section 3.1.2, we have expressed a concern on the feasibility of the steering maneuver for low speed due to the steering wheel angle's physical limitation, for Volvo XC90, ±720°. These findings are directly in line with our previous analysis and justify why we have discarded speeds below 20kph from the analysis for the steering maneuver. The second finding is that a lateral acceleration of $1g$ is not always reached while following the desired path generated on that assumption.

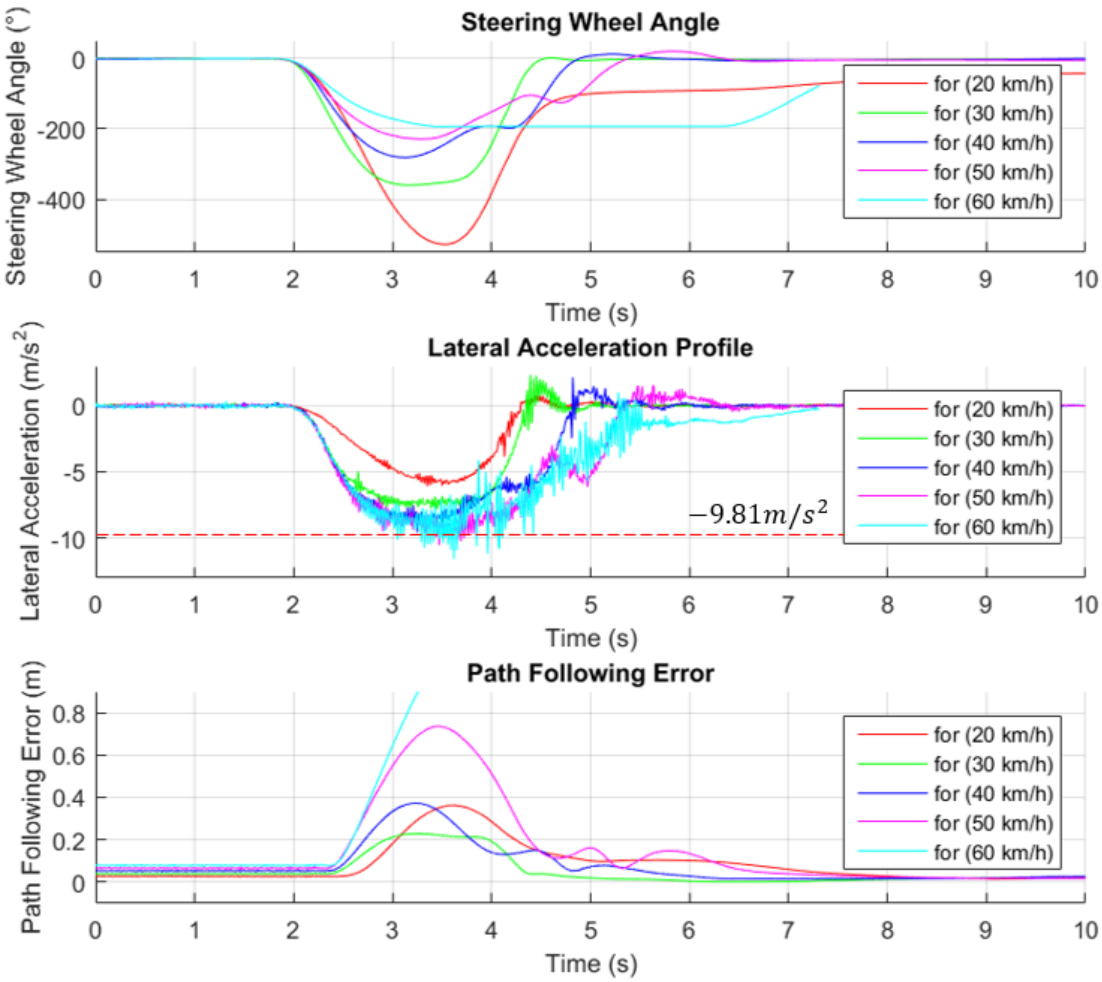

Figure 5.6: *Steering Maneuver Results for speed range [20kph, 60kph]*

In Figure 5.7, we illustrate the desired and actual path for a test performed at 40kph in order to visualize an example of the path following error.

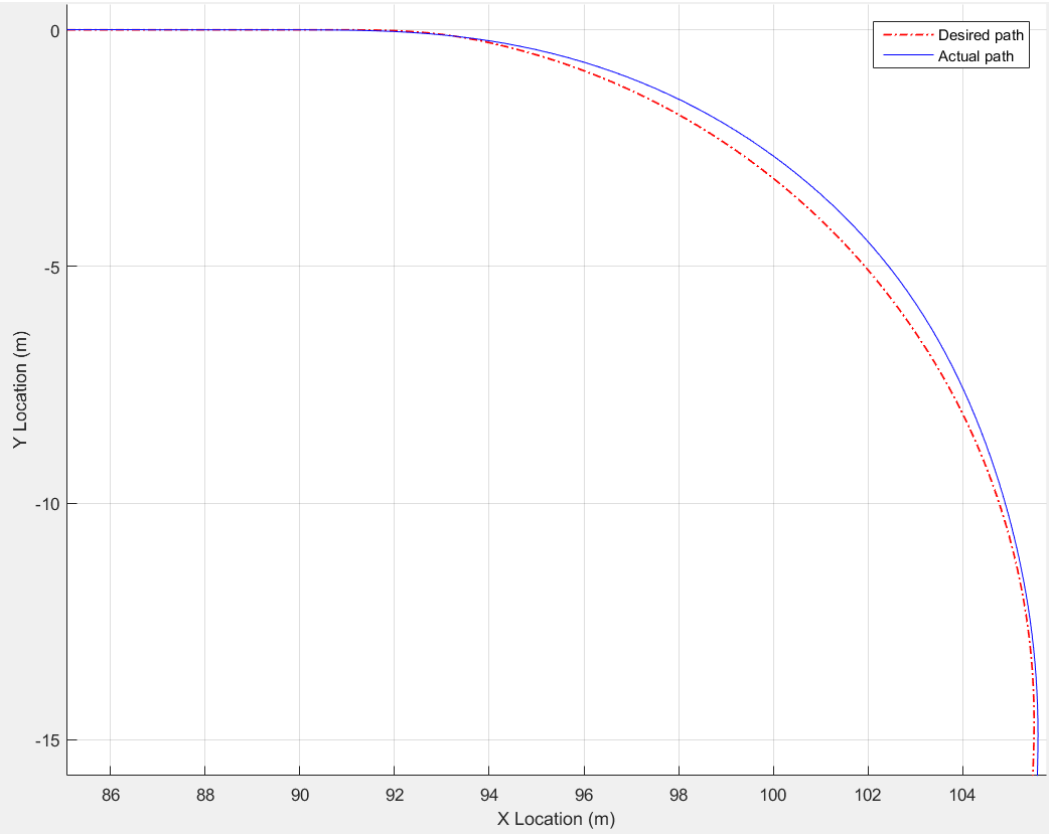

***Figure** 5.7: Desired vs Actual Trajectories for 40kph*

Further experiments have been carried out to investigate if the vehicle has drifted at 60kph because of the high level of lateral acceleration required to keep the vehicle on the desired path. Therefore, we have generated trajectories at this exact speed decreasing the assumed maximum lateral acceleration to $0.9g$, $0.8g$, and $0.7g$. The vehicle had successfully followed all generated paths with a path following error less than 1m. Results are illustrated in Figure 5.8 and lead to conclude that for the same speed the path following error decreases for trajectories that require lower levels of lateral acceleration.

We took benefit of these interesting facts revealed by the experimental results to tune the maximum lateral acceleration parameter. We fixed a goal which is to guarantee a maximum path following error equal to 0.55m, see Figure 5.8. Thus, the supervisor will adjust the value of the lateral acceleration used to generate safe trajectories according to the given speed. We use $1g$ for speeds $\in$ [20kph, 50kph[and $0.7g$ for speeds $\in$ [50kph, 60kph].

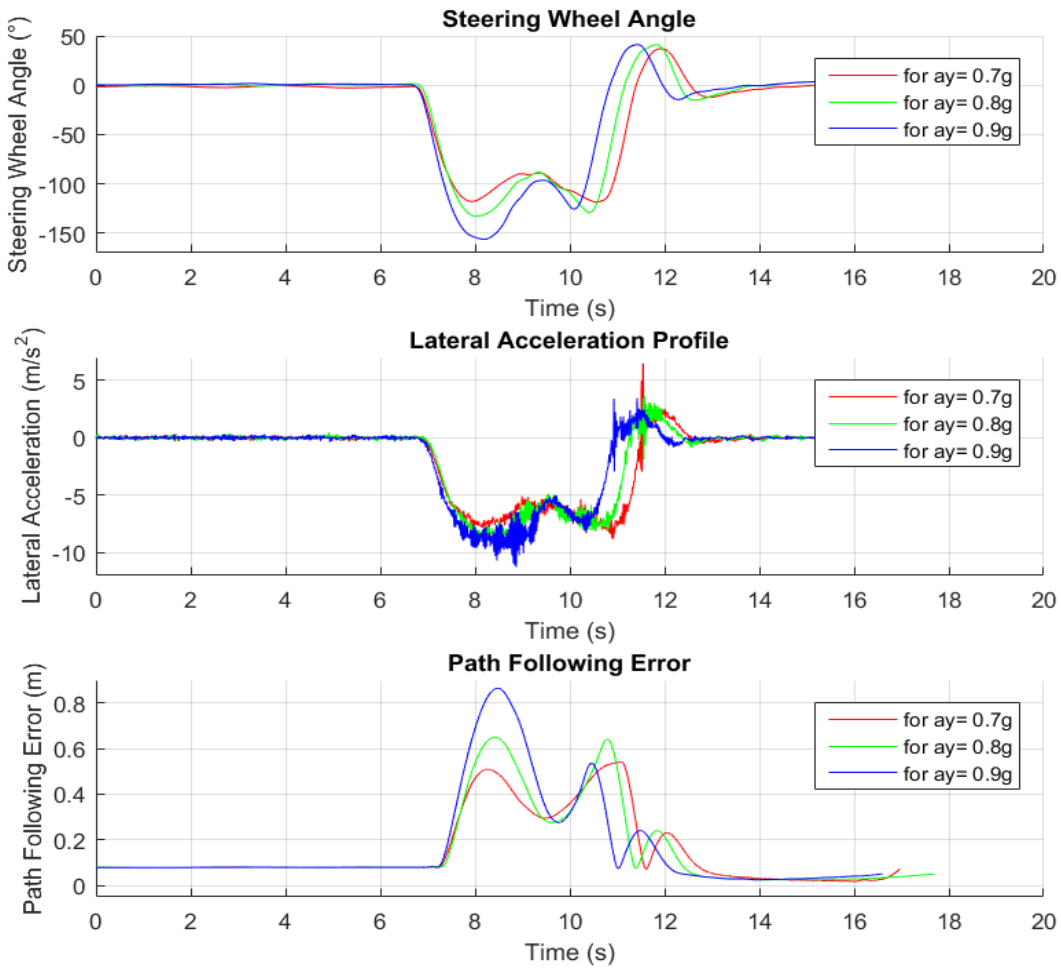

Figure 5.8: *Steering Maneuver Results for 60kph*

5.3 Braking Maneuver Validation

Collision-free braking-based trajectories were generated for a speed range between 20kph and 60kph with increments of 10kph. The trajectory is comprised of 2 portions: drive straight with constant speed until reaching the last point to brake then braking with maximum deceleration assumed to be $0.8g$, see Figure 5.9. Maneuver-based trajectory generation is explained in section 3.4. The validation of the braking maneuver is done following exactly the same steps as for validation of the steering maneuver.

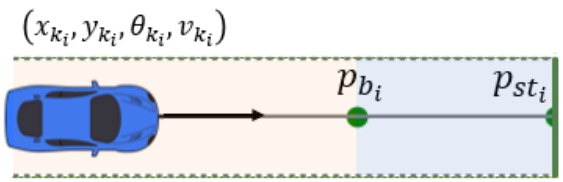

Figure 5.9: *Trajectory generation for a Braking Maneuver.*
Vehicles drive straight in the orange zone, and brake in the blue zone.

The vehicle has successfully followed the given collision-free paths for speeds between 20kph and 60kph with a path following error less than 0.5m, see Figure 5.9.

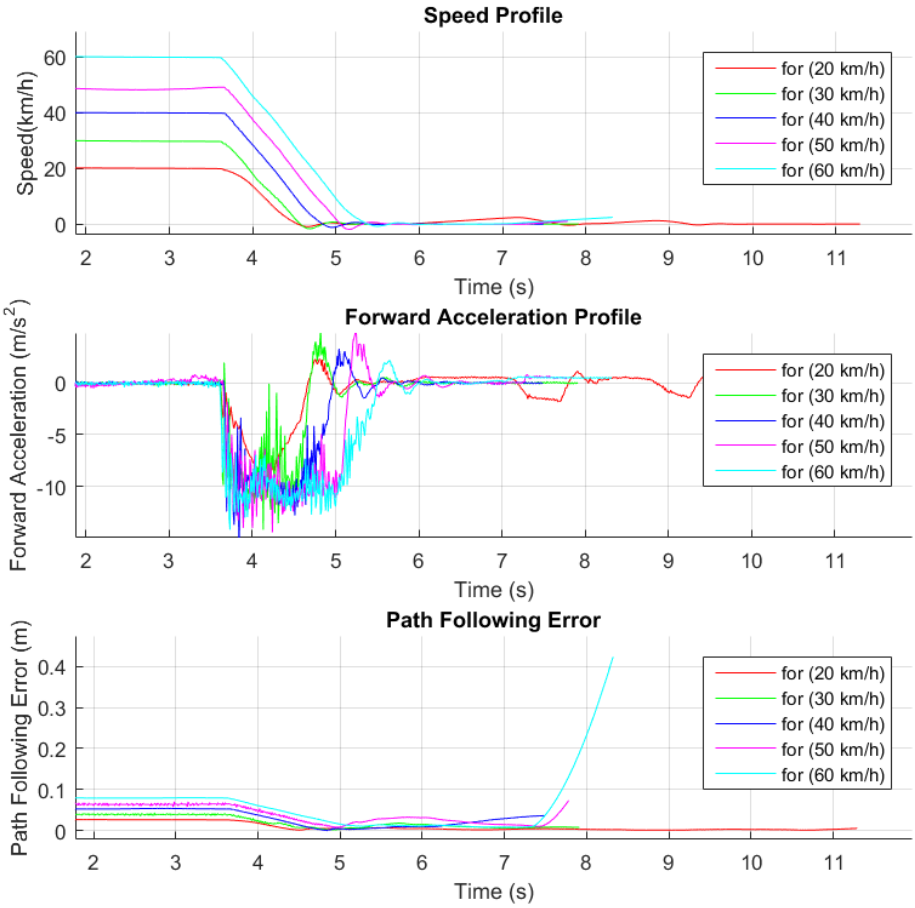

Figure 5.10: *Braking Maneuver Results for speed range [20kph, 60kph]*

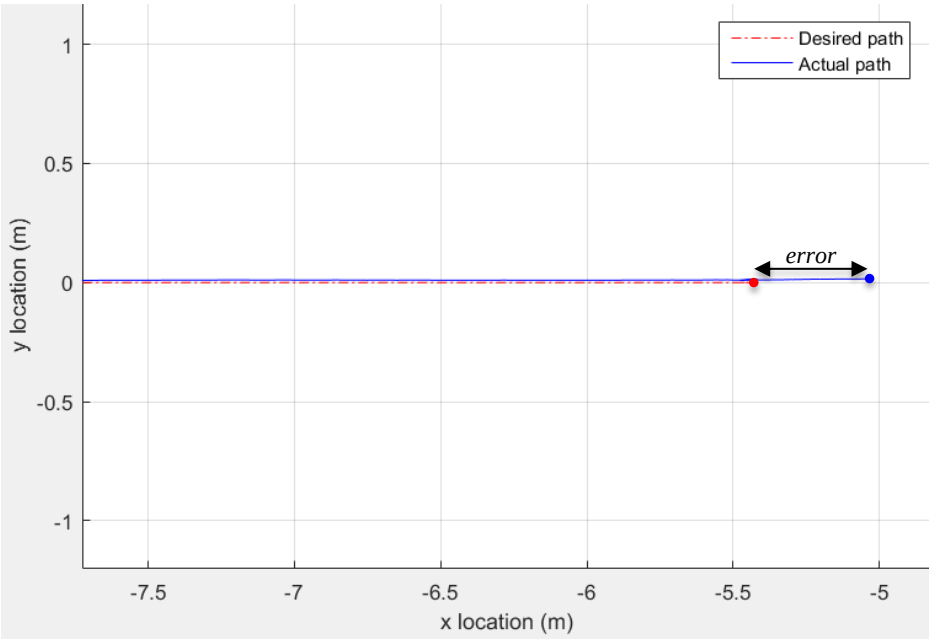

Figure 5.11: *Desired vs Actual Trajectories for 60kph*

From these results, it is clear that the path following error slightly increases with the speed. It is notable that the main error resides in the last few seconds of the test, see Figure 5.10. This finding reflects that the vehicle does not stop at the desired stop point, see Figure 5.11. This error is due to the path following controller. The braking maneuver was generated based on achieving a deceleration of $0.8g$. In Figure 5.10, we see that the vehicle does not respect the assumed value and applies a deceleration of $1.2g$. Consequently, the vehicle stops before the desired stop point and keeps accelerating and decelerating afterwards to reach the predefined stop point.

While developing our safety maneuvers, we assumed that the stop point will be respected. Hence, we have reviewed the braking maneuvers in order to verify the influence of such error. Brake – Brake Maneuver was safe as the stop points were defined either outside the collision area or one outside and the other inside, see section 3.2. Concerning, Steer – Brake Maneuver, risks only came out for the clockwise steering approach since for the other approach the safe trajectories never intersect, see section 3.3. A modification was absolutely needed to overcome this safety threat. Therefore, we translated the stop point 1m behind the original stop point as shown in figure 5.12. This safe margin is sufficient to account for the path following error observed in Figure 5.10 and it corresponds to the same value defined for the safety margin in the lateral direction. This adjustment ensures that the vehicle performing the braking maneuver will never collide with the vehicle performing the steering maneuver.

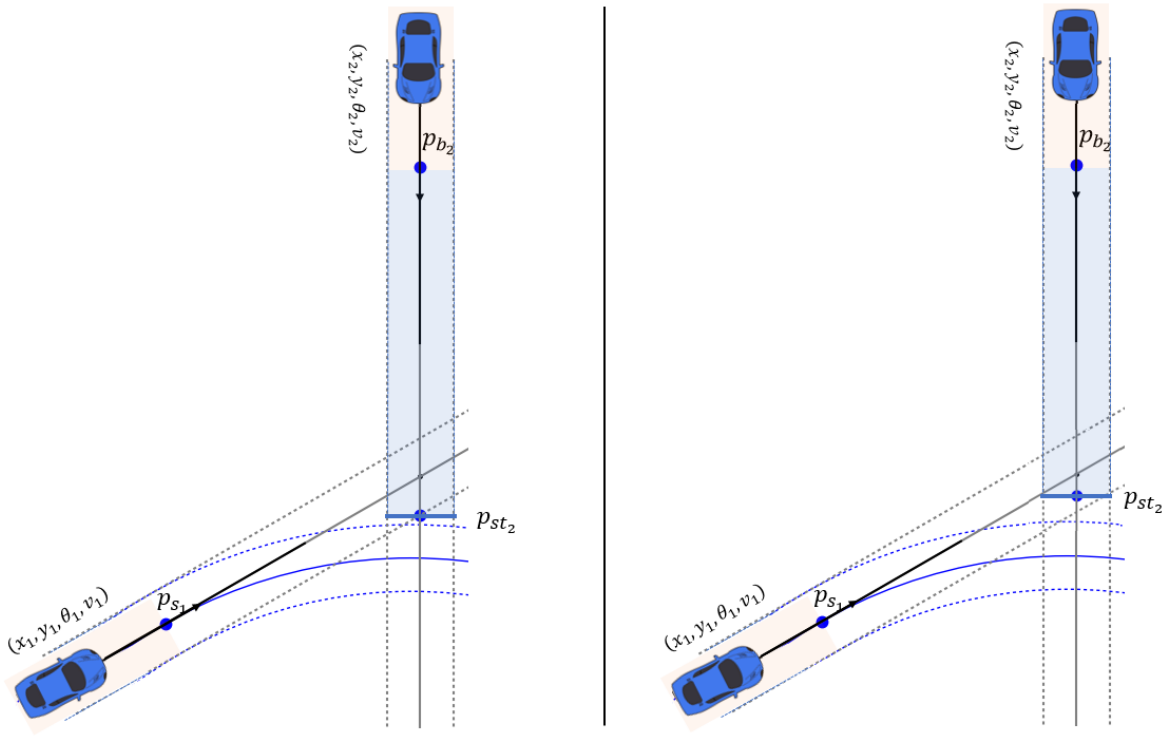

Figure 5.12: *Maneuver before modification on the left, Maneuver after modification on the right*

5.4 Supervisor Re-evaluation

This section summarizes the findings and contributions made in this thesis work. Previously in section 4.2, we have evaluated and defined the benchmark behaviour of the supervisor module based on the average time-to-collision (TTC) at each collision angle. This criterion reflects how far the vehicles are from the collision center at the activation of the safe trajectories. A re-evaluation was required to highlight the deviation from the benchmark after tuning the maximum lateral acceleration and editing the Steer – Brake Maneuver. Nevertheless, when comparing the following results to those presented in section 4.2, it can be concluded that the actual supervisor's behaviour slightly diverts from the benchmark, see Figure 5.13. The main conclusion that can be drawn is that, despite of this deviation, we on average activate the collision-free trajectories 1s before collisions occur. This obtained performance is quite satisfying since usually the threshold used by some collision-mitigation systems for autonomous driving is 1s [5]. Therefore, all last points to react with a time to collision less than 1s will allow to test some autonomous driving functionalities. However, less conservative safety maneuvers can be developed to improve the performance of the supervisor module for collision angles that lead to an Average TTC larger than 1s.

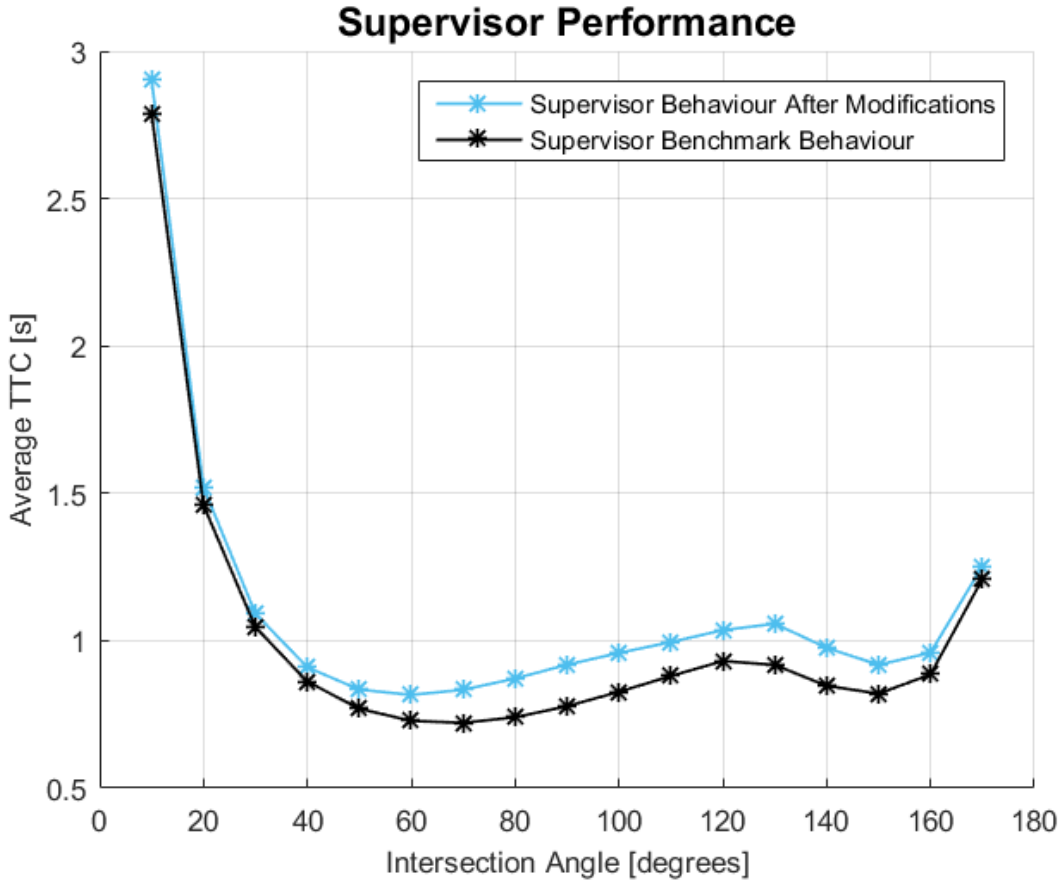

Figure 5.13: SupervisorPerformance after modifications

The curves illustrate the performance of the supervisor module in aborting the test case by applying the optimal safety maneuver before and after modifications. The average TTC is computed from the TTCs obtained for scenarios with a specific intersection angle but with various combinations of driving speeds. TTC refers to the time it would take the vehicles to reach the collison center from the last point to react if the vehicles would have kept constant speed.

For the sake of brevity, optimal safety maneuver heat maps for each collision angle $\varphi \in]0°, 180°[$ were regenerated after incorporating the modifications in the supervisor and they are given in Appendix II.

6 Conclusion and Future Works

We have presented a functional architecture of a supervisor module to be implemented in a robotized vehicle in the loop (VIL) framework for autonomous driving (AD) verification. The supervisor module has two crucial roles. Monitoring the test objects for collision detection and performing an emergency action when a dangerous situation arises. We have evaluated and validated its performance for an angled collision application and a range of speed between 20kph and 60kph.

A deterministic approach is chosen to be developed for collision detection to avoid computational complexity in real-time implementation, an essential aspect of our study to overcome the issues encountered in related work [10]. Based on vehicles' given states, future trajectories have been estimated by applying a linear extrapolation method. On the other hand, the collision threat assessment has been measured by evaluating vehicles' occupancy time of the collision area.

Three safety maneuvers are developed for collision avoidance based on geometrical approaches and a desired vehicle's motion taking into account physical constraints such as maximum lateral acceleration and deceleration. Each maneuver is defined by its last point to react according to a steering or braking action. If the vehicles cross this point, no feasible maneuver can prevent a collision from occurring. This criterion allows the supervisor to declare an emergency and select the optimal safety maneuver to be performed for collision avoidance.

The last point to react approach has been validated by performing a set of experiments on a Volvo XC90 equipped with the driving robot that will be used in the vehicle in the loop (VIL) framework. The obtained results confirm that the supervisor can effectively guarantee a safe exit for the majority of the studied scenarios with an emergency intervention 1s before collision.

Ideally, these findings should be replicated in a study where the boundaries of the road are taking into account. Nevertheless, designing new safety maneuvers could fruitfully improve the performance of the supervisor module. For example, scrutinizing how one vehicle can adapt its velocity based on that of the other to avoid overlapping.

Moreover, higher robustness of the collision detection module can be attained by adding uncertainties on acceleration and vehicles' states measurements. Such probabilistic approach may lead to a computational burden for the real-time implementation. This is an issue for future research to explore.

At last, we finally highlight that, our proposed supervisor module is a convenient solution for safety decision-making in a vehicle in the loop framework, which ensures the safe execution of the test case and requires very modest computational power suitable for real-time implementation.

References

1. *World Health Organization: Road traffic injuries. <https://www.who.int/violence_injury_prevention/road_traffic/en/>, accessed 30 May 2019.*
2. *European Commission, (2019): Intelligent transport systems. <https://ec.europa.eu/transport/themes/its/road_en>, accessed 12 May 2019.*
3. *Volvo Cars, (2009): 3-point safety belt from Volvo - the most effective lifesaver in traffic for fifty years. <https://www.media.volvocars.com/global/en-gb/media/pressreleases/18405> accessed 30 May 2019.*
4. *L. Bjlkeflo, R. Laxing, M. Djup, P. Gustafsson, R Gustafsson, N. Lundin, V. Johansson, V. Naterjee, J. Pohl, E. Schiller, and B. J. Svensson (2018): CHRONOS Part 1, 2016-02573 External report. <https://www.vinnova.se/contentassets/3f1ea323948d43ce90732c74dc10fd19/2016-02573.pdf> accessed 20 April 2019.*
5. *S. Glaser, B. Vanholme, S. Mammar, D. Gruyer, and L. Nouveliere, (2010): Maneuver-based trajectory planning for highly autonomous vehicles on real road with traffic and driver interaction. IEEE Trans. Intell. Transp. Syst., vol. 11, no. 3, pp. 589–606, 2010.*
6. *J. Shah, M. Best, A. Benmimoun, and M. L. Ayat, (2015): Autonomous rear-end collision avoidance using an electric power steering system. Proc IMechE Part D: J Automobile Engineering 2015, Vol. 229(12) 1639-1655.*
7. *S. Noh, (2018): Probabilistic Collision Threat Assessment for Autonomous Driving at Road Intersections Inclusive of Vehicles in Violation of Traffic Rules. IEEE/RSJ International Conference on Intelligent Robots and Systems (IROS), 2018.*
8. *J. Kim, (2018): Collision Risk Assessment Algorithm via Lane-Based Probabilistic Motion Prediction of Surrounding Vehicles. IEEE Trans. Intell. Transp. Syst., vol. 19, no. 9, September 2018.*
9. *J. Kim, and D. Kum, (2018): Threat Prediction Algorithm based on Local Path Candidates and Surrounding Vehicle Trajectory Predictions for Automated Driving Vehicles. IEEE Intelligent Vehicles Symposium, 2018.*
10. *A. Hahlin, and A. Olsson, (2017): Centralized collision avoidance system for automated vehicles. Master's thesis, Departement of Electrical Engineering, Chalmers University of Technology, Göteborg, Sweden, 2017, 69 pp.*
11. *M. Likhachev, D. Ferguson, G. Gordon, A. Stentz, and S. Thrun (2001): Anytime Dynamic A *: An Anytime, Replanning Algorithm.*
12. *S. M. LaValle, (1998): Rapidly-Exploring Random Trees: A New Tool for Path-Planning.*
13. *O. Khatib, (1985): Real-Time obstacle avoidance for manipulators and mobile robots. ,Tech. rep. Artificial Intelligence Laboratory, Stanford University, Stanford, CA 94305, pp. 500–505, 1985.*
14. *N. Murgovski, G. Rodrigues de Campos, and J. Sjöberg, (2015): Convex modelling of conflict resolution at traffic intersections. IEEE 54th Annual Conference on Decision and Control (CDC), 2015.*

15. *J. Karlsson, N. Murgovski, and J. Sjöberg, (2016): Temporal vs. spatial formulation of autonomous overtaking algorithms. IEEE 19th International Conference on Intelligent Transportation Systems (ITSC), 2016.*
16. *L. Riegger, M. Carlander, N. Lidander, N. Murgovski, and J. Sjöberg, (2016): Centralized MPC for Autonomous Intersection Crossing. IEEE 19th International Conference on Intelligent Transportation Systems (ITSC), 2016.*
17. *J. Van Den Berg, S. J. Guy, M. Lin, and D. Manocha, (2012): Reciprocal collision avoidance for multiple mobile robots. IEEE International Conference on Robotics and Automation, pp. 1–16, 2012.*
18. *D. Johansson, (2019): Dynamic Path Planning for collision avoidance in a robotized framework for autonomous driving verification. Master's Thesis, Department of Automatic Control, Lund University, Göteborg, Sweden, 2019, 95 pp.*

Appendix

I. Safety Maneuver Comparison

Steer – Steer Maneuver	*Brake – Brake Maneuver*	*Steer – Brake Maneuver*
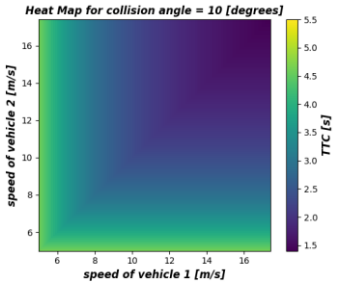	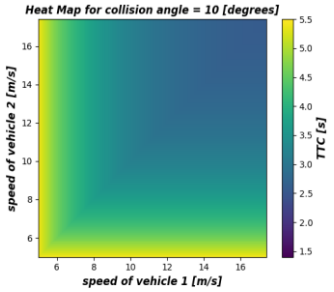	X
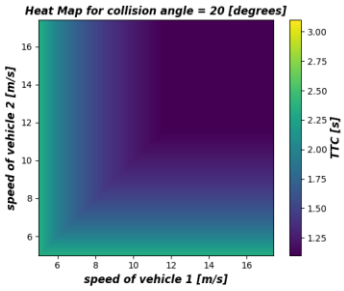	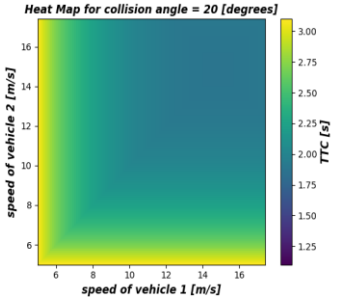	X
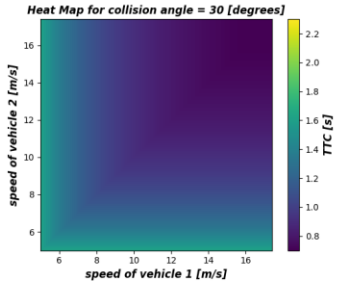	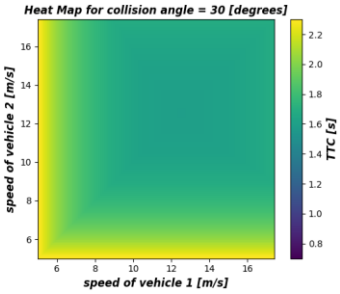	X
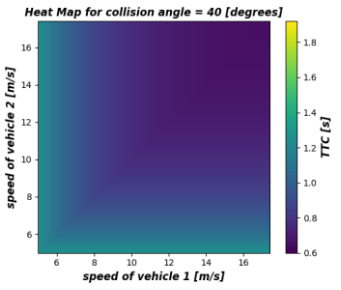	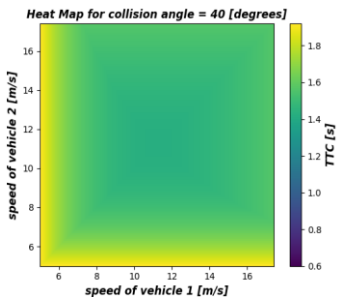	X
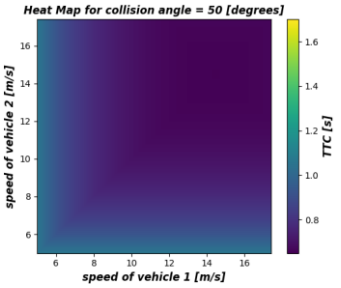	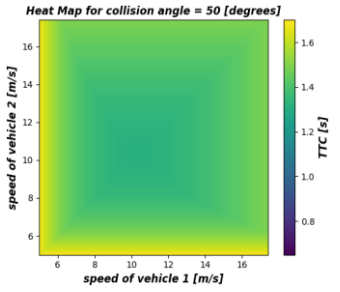	X

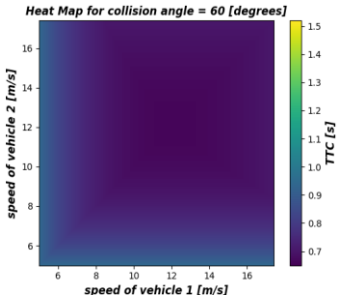
Heat Map for collision angle = 60 [degrees]
speed of vehicle 2 [m/s]
speed of vehicle 1 [m/s]
TTC [s]

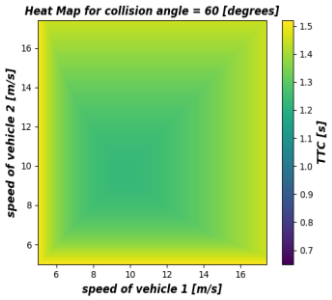
Heat Map for collision angle = 60 [degrees]
speed of vehicle 2 [m/s]
speed of vehicle 1 [m/s]
TTC [s]

X

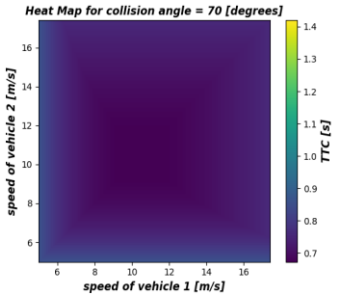
Heat Map for collision angle = 70 [degrees]
speed of vehicle 2 [m/s]
speed of vehicle 1 [m/s]
TTC [s]

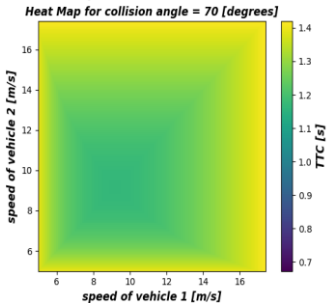
Heat Map for collision angle = 70 [degrees]
speed of vehicle 2 [m/s]
speed of vehicle 1 [m/s]
TTC [s]

X

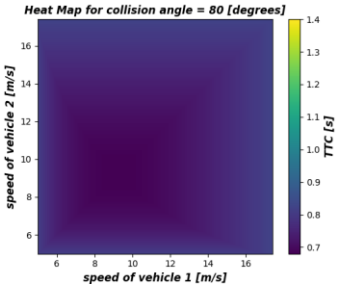
Heat Map for collision angle = 80 [degrees]
speed of vehicle 2 [m/s]
speed of vehicle 1 [m/s]
TTC [s]

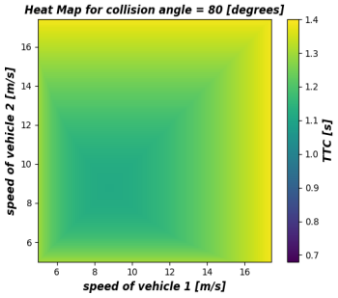
Heat Map for collision angle = 80 [degrees]
speed of vehicle 2 [m/s]
speed of vehicle 1 [m/s]
TTC [s]

X

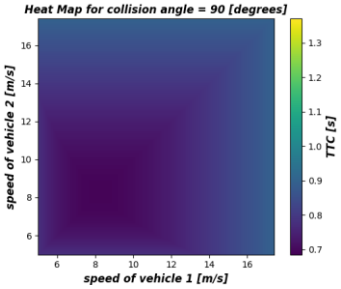
Heat Map for collision angle = 90 [degrees]
speed of vehicle 2 [m/s]
speed of vehicle 1 [m/s]
TTC [s]

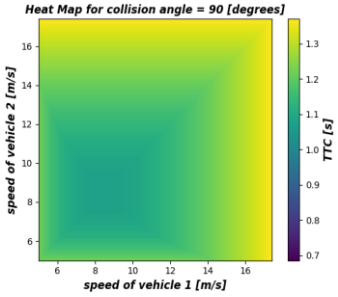
Heat Map for collision angle = 90 [degrees]
speed of vehicle 2 [m/s]
speed of vehicle 1 [m/s]
TTC [s]

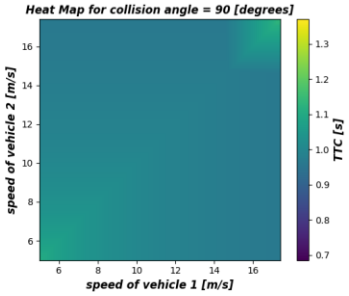
Heat Map for collision angle = 90 [degrees]
speed of vehicle 2 [m/s]
speed of vehicle 1 [m/s]
TTC [s]

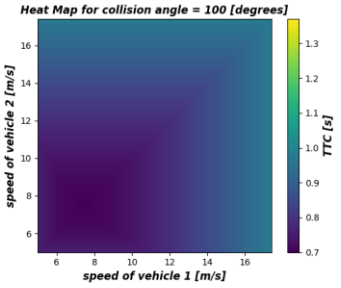
Heat Map for collision angle = 100 [degrees]
speed of vehicle 2 [m/s]
speed of vehicle 1 [m/s]
TTC [s]

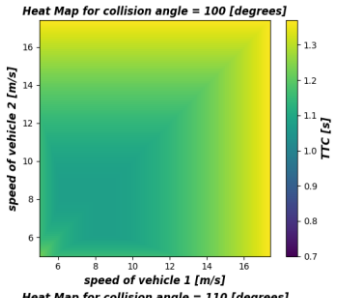
Heat Map for collision angle = 100 [degrees]
speed of vehicle 2 [m/s]
speed of vehicle 1 [m/s]
TTC [s]

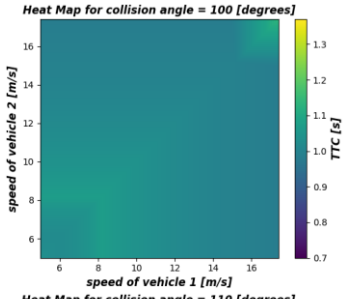
Heat Map for collision angle = 100 [degrees]
speed of vehicle 2 [m/s]
speed of vehicle 1 [m/s]
TTC [s]

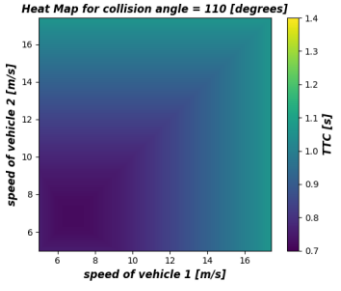
Heat Map for collision angle = 110 [degrees]
speed of vehicle 2 [m/s]
speed of vehicle 1 [m/s]
TTC [s]

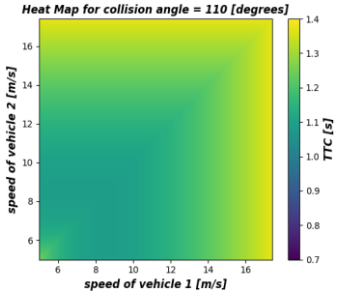
Heat Map for collision angle = 110 [degrees]
speed of vehicle 2 [m/s]
speed of vehicle 1 [m/s]
TTC [s]

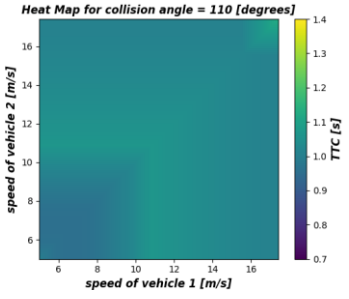
Heat Map for collision angle = 110 [degrees]
speed of vehicle 2 [m/s]
speed of vehicle 1 [m/s]
TTC [s]

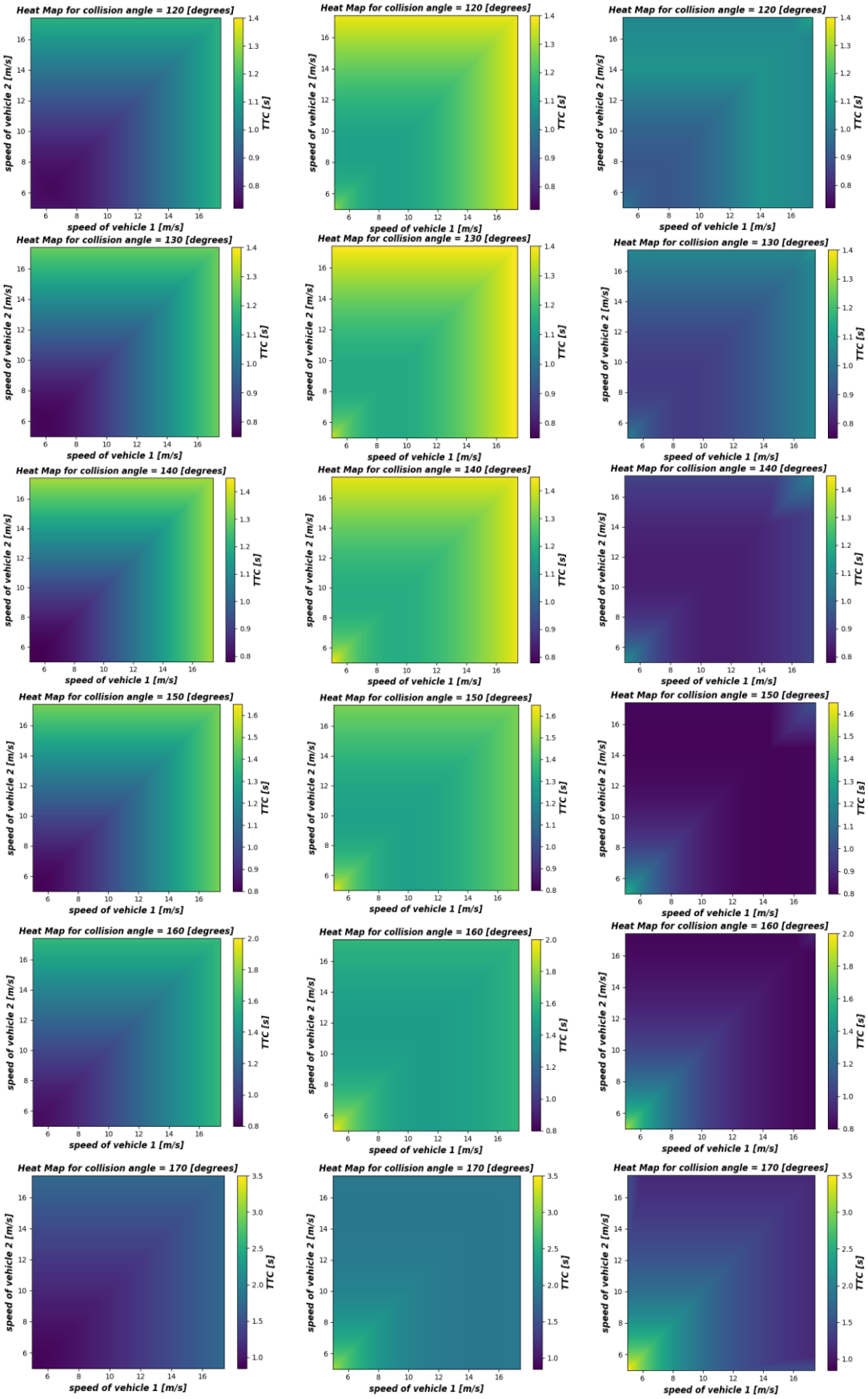
Heat Map for collision angle = 120 [degrees]
Heat Map for collision angle = 120 [degrees]
Heat Map for collision angle = 120 [degrees]
Heat Map for collision angle = 130 [degrees]
Heat Map for collision angle = 130 [degrees]
Heat Map for collision angle = 130 [degrees]
Heat Map for collision angle = 140 [degrees]
Heat Map for collision angle = 140 [degrees]
Heat Map for collision angle = 140 [degrees]
Heat Map for collision angle = 150 [degrees]
Heat Map for collision angle = 150 [degrees]
Heat Map for collision angle = 150 [degrees]
Heat Map for collision angle = 160 [degrees]
Heat Map for collision angle = 160 [degrees]
Heat Map for collision angle = 160 [degrees]
Heat Map for collision angle = 170 [degrees]
Heat Map for collision angle = 170 [degrees]
Heat Map for collision angle = 170 [degrees]
speed of vehicle 1 [m/s]
speed of vehicle 2 [m/s]
TTC [s]

II. Supervisor Performance

Supervisor performance regarding the activation of the optimal safety maneuver
+ = Steer - Steer Maneuver
x = Brake - Brake Maneuver
● = Steer - Brake Maneuver

Benchmark Behaviour | ***Behaviour After Modifications***

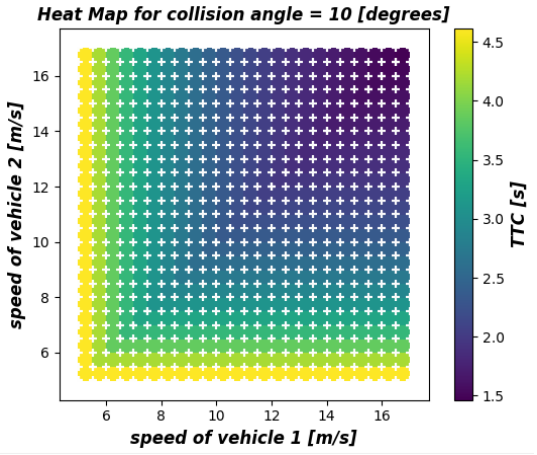

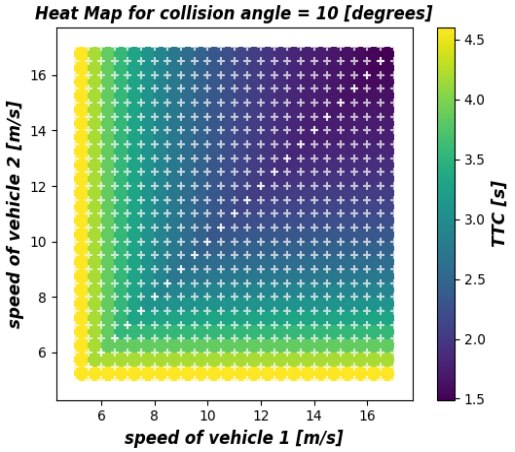

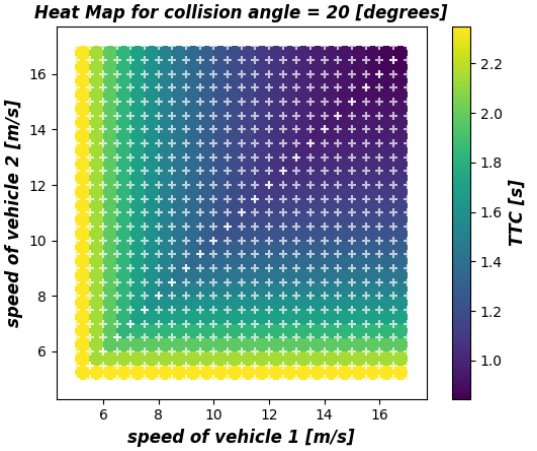

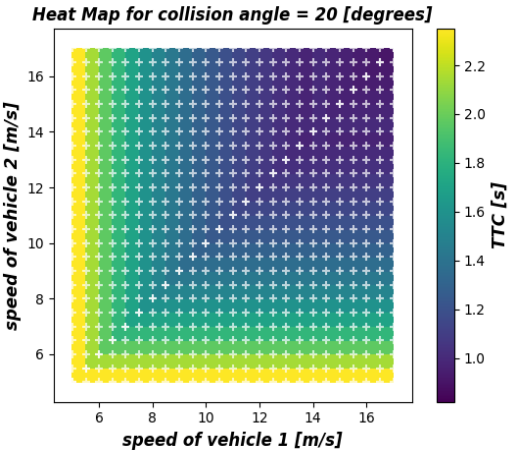

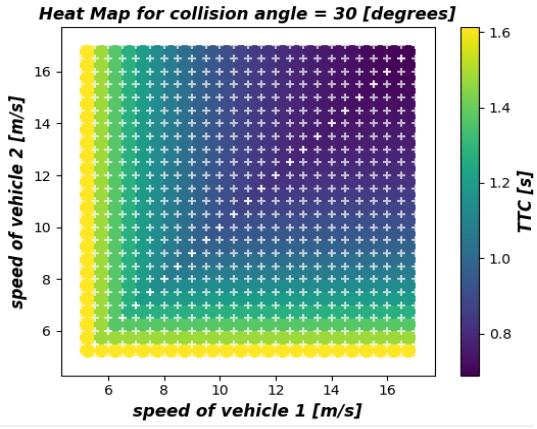

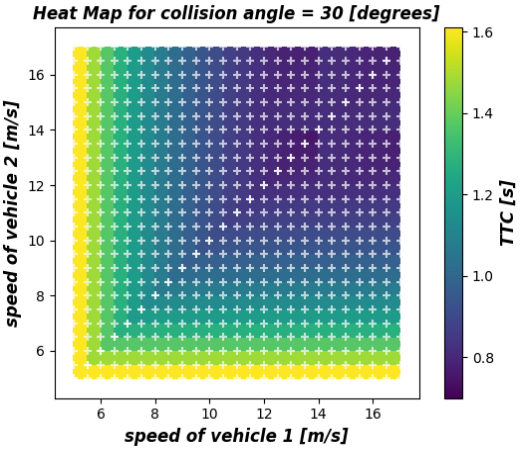

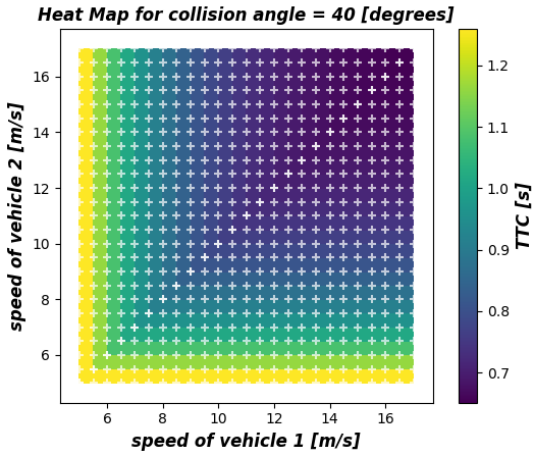
Heat Map for collision angle = 40 [degrees]
speed of vehicle 2 [m/s]
speed of vehicle 1 [m/s]
TTC [s]

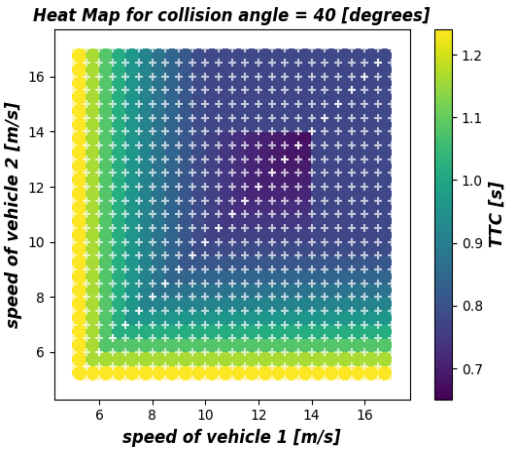
Heat Map for collision angle = 40 [degrees]
speed of vehicle 2 [m/s]
speed of vehicle 1 [m/s]
TTC [s]

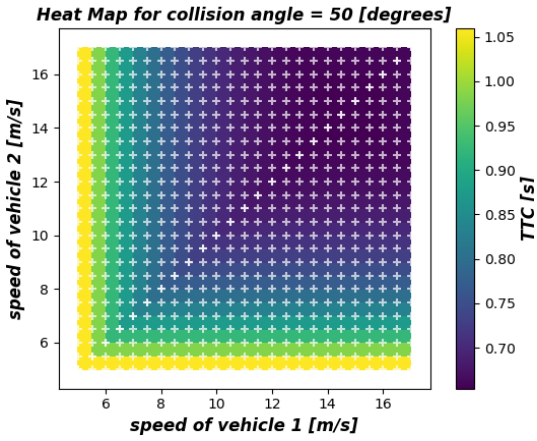
Heat Map for collision angle = 50 [degrees]
speed of vehicle 2 [m/s]
speed of vehicle 1 [m/s]
TTC [s]

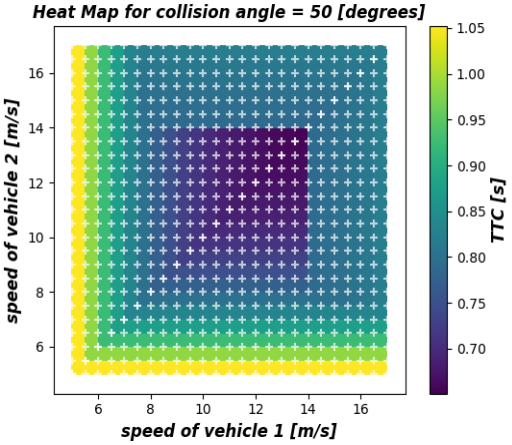
Heat Map for collision angle = 50 [degrees]
speed of vehicle 2 [m/s]
speed of vehicle 1 [m/s]
TTC [s]

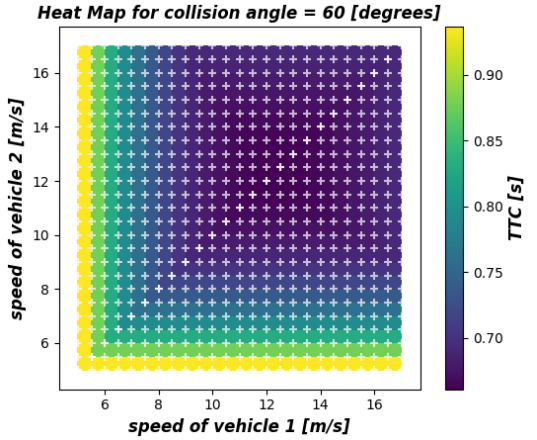
Heat Map for collision angle = 60 [degrees]
speed of vehicle 2 [m/s]
speed of vehicle 1 [m/s]
TTC [s]

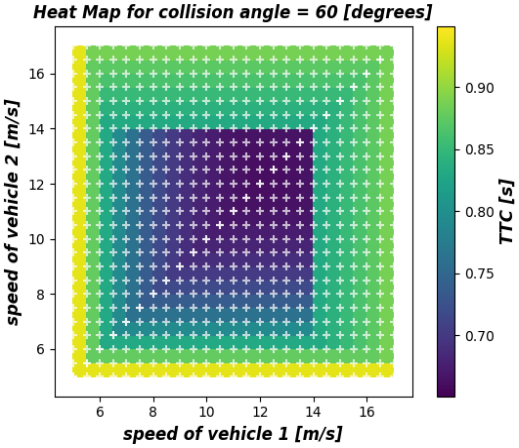
Heat Map for collision angle = 60 [degrees]
speed of vehicle 2 [m/s]
speed of vehicle 1 [m/s]
TTC [s]

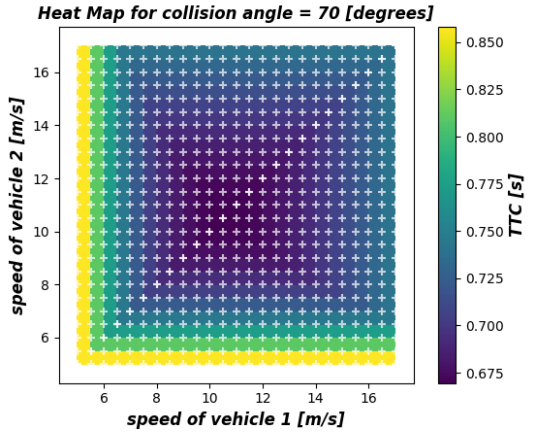
Heat Map for collision angle = 70 [degrees]
speed of vehicle 2 [m/s]
speed of vehicle 1 [m/s]
TTC [s]

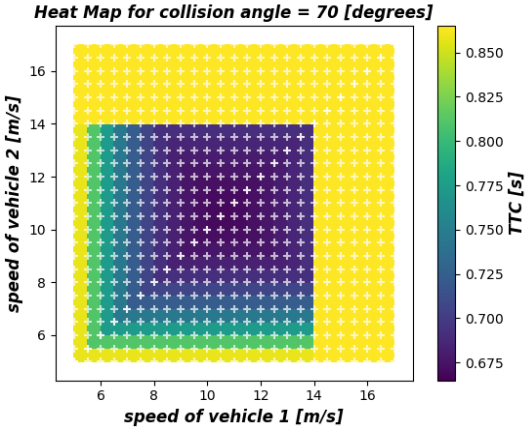
Heat Map for collision angle = 70 [degrees]
speed of vehicle 2 [m/s]
speed of vehicle 1 [m/s]
TTC [s]

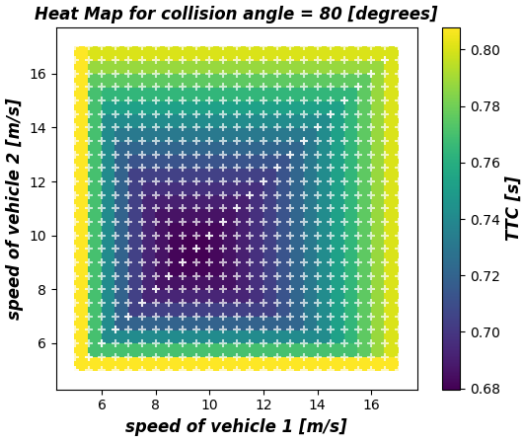
Heat Map for collision angle = 80 [degrees]
speed of vehicle 2 [m/s]
speed of vehicle 1 [m/s]
TTC [s]

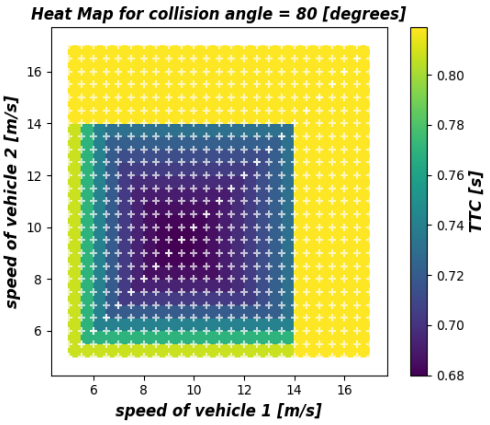
Heat Map for collision angle = 80 [degrees]
speed of vehicle 2 [m/s]
speed of vehicle 1 [m/s]
TTC [s]

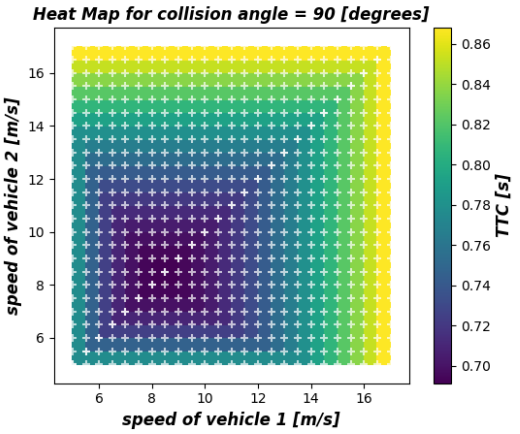
Heat Map for collision angle = 90 [degrees]
speed of vehicle 2 [m/s]
speed of vehicle 1 [m/s]
TTC [s]

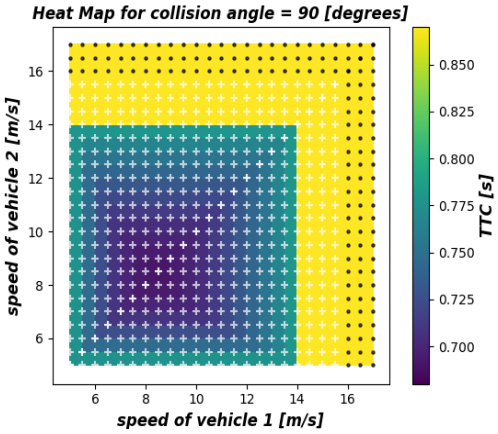
Heat Map for collision angle = 90 [degrees]
speed of vehicle 2 [m/s]
speed of vehicle 1 [m/s]
TTC [s]

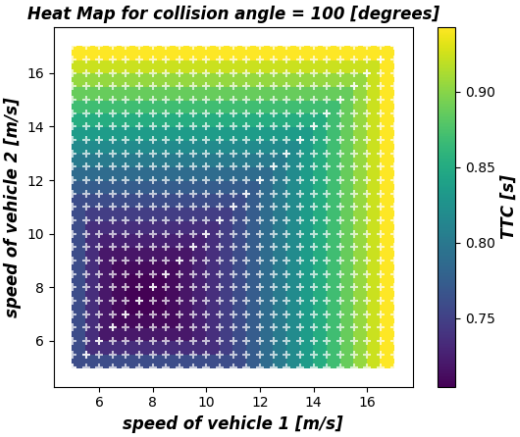
Heat Map for collision angle = 100 [degrees]
speed of vehicle 2 [m/s]
speed of vehicle 1 [m/s]
TTC [s]

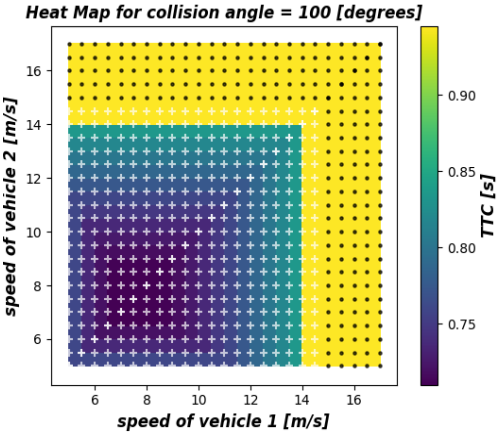
Heat Map for collision angle = 100 [degrees]
speed of vehicle 2 [m/s]
speed of vehicle 1 [m/s]
TTC [s]

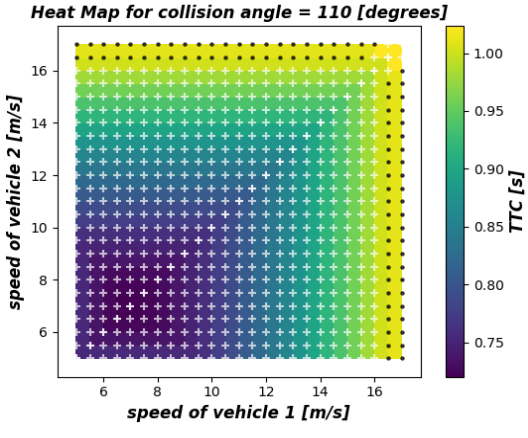
Heat Map for collision angle = 110 [degrees]
speed of vehicle 2 [m/s]
speed of vehicle 1 [m/s]
TTC [s]

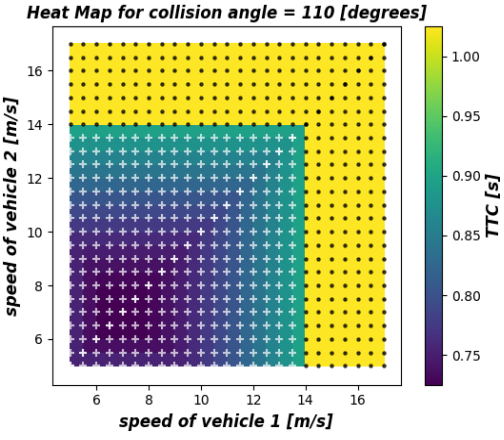
Heat Map for collision angle = 110 [degrees]
speed of vehicle 2 [m/s]
speed of vehicle 1 [m/s]
TTC [s]

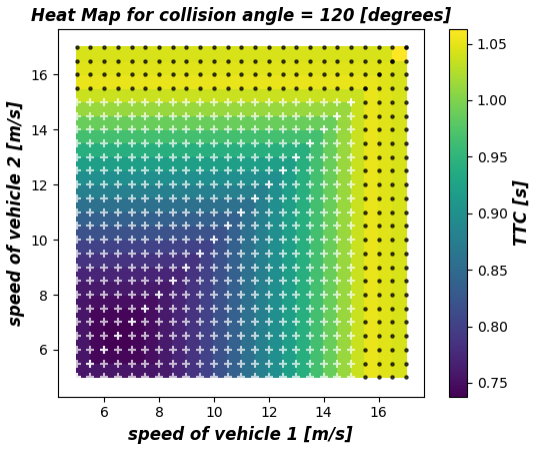
Heat Map for collision angle = 120 [degrees]
speed of vehicle 2 [m/s]
speed of vehicle 1 [m/s]
TTC [s]

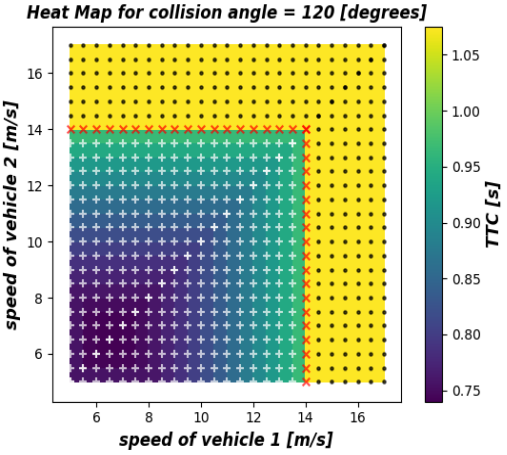
Heat Map for collision angle = 120 [degrees]
speed of vehicle 2 [m/s]
speed of vehicle 1 [m/s]
TTC [s]

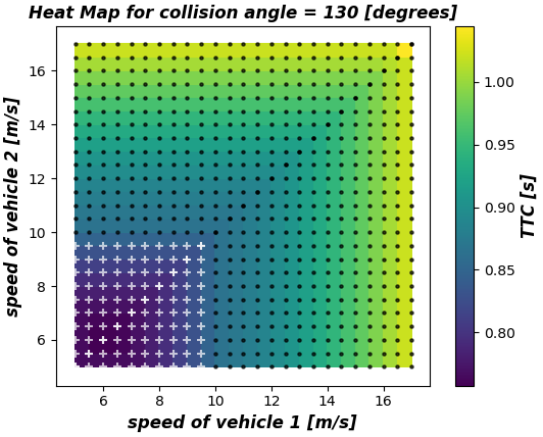
Heat Map for collision angle = 130 [degrees]
speed of vehicle 2 [m/s]
speed of vehicle 1 [m/s]
TTC [s]

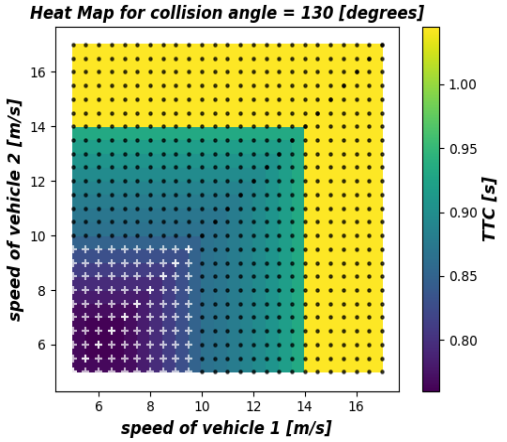
Heat Map for collision angle = 130 [degrees]
speed of vehicle 2 [m/s]
speed of vehicle 1 [m/s]
TTC [s]

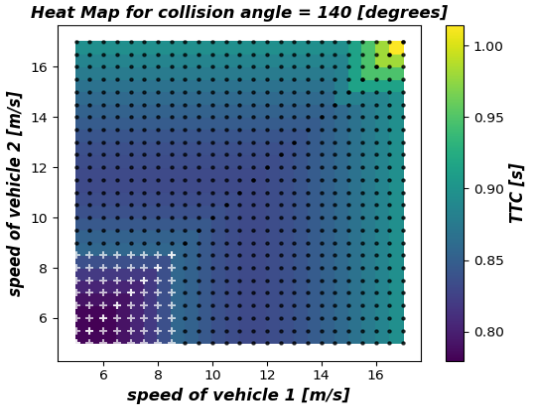
Heat Map for collision angle = 140 [degrees]
speed of vehicle 2 [m/s]
speed of vehicle 1 [m/s]
TTC [s]

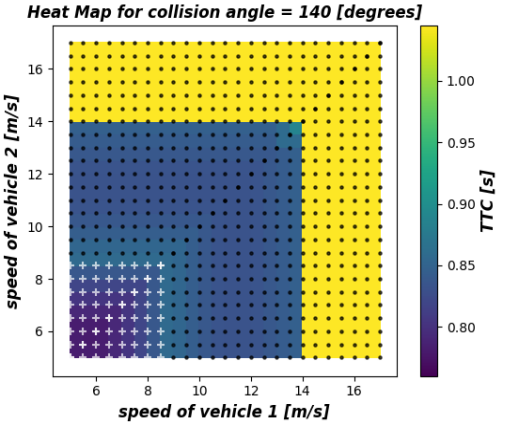
Heat Map for collision angle = 140 [degrees]
speed of vehicle 2 [m/s]
speed of vehicle 1 [m/s]
TTC [s]

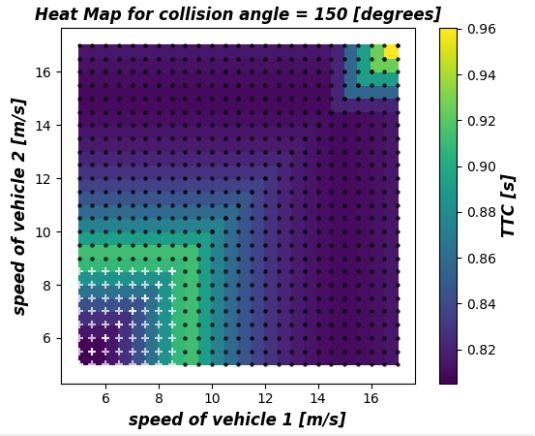
Heat Map for collision angle = 150 [degrees]
speed of vehicle 2 [m/s]
speed of vehicle 1 [m/s]
TTC [s]

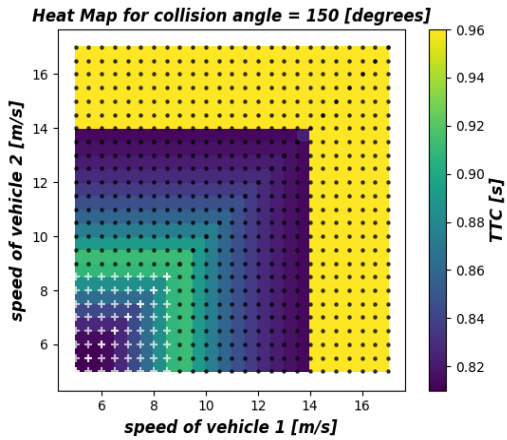
Heat Map for collision angle = 150 [degrees]
speed of vehicle 2 [m/s]
speed of vehicle 1 [m/s]
TTC [s]

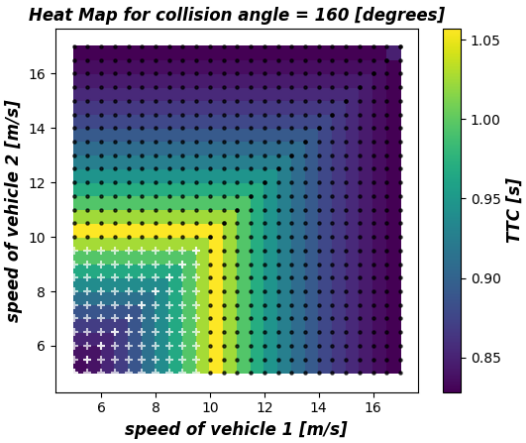
Heat Map for collision angle = 160 [degrees]
speed of vehicle 2 [m/s]
speed of vehicle 1 [m/s]
TTC [s]
6
8
10
12
14
16
0.85
0.90
0.95
1.00
1.05

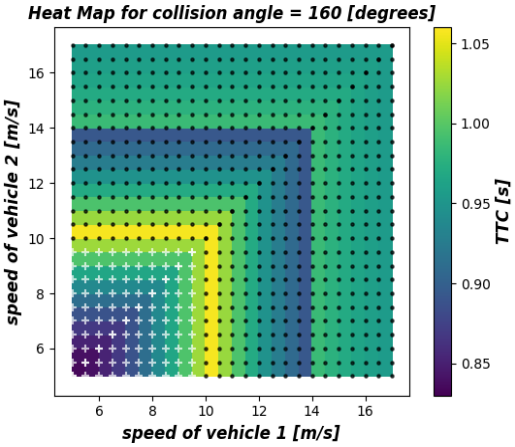
Heat Map for collision angle = 160 [degrees]
speed of vehicle 2 [m/s]
speed of vehicle 1 [m/s]
TTC [s]
6
8
10
12
14
16
0.85
0.90
0.95
1.00
1.05

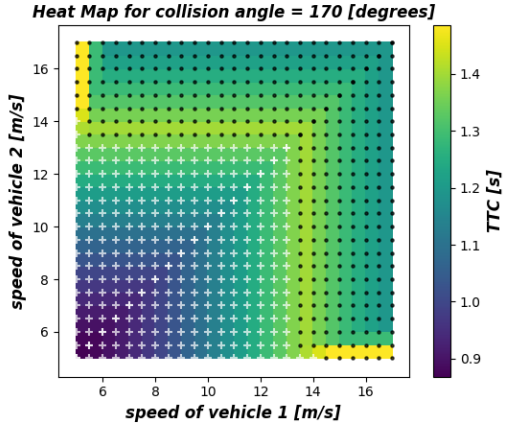
Heat Map for collision angle = 170 [degrees]
speed of vehicle 2 [m/s]
speed of vehicle 1 [m/s]
TTC [s]
6
8
10
12
14
16
0.9
1.0
1.1
1.2
1.3
1.4

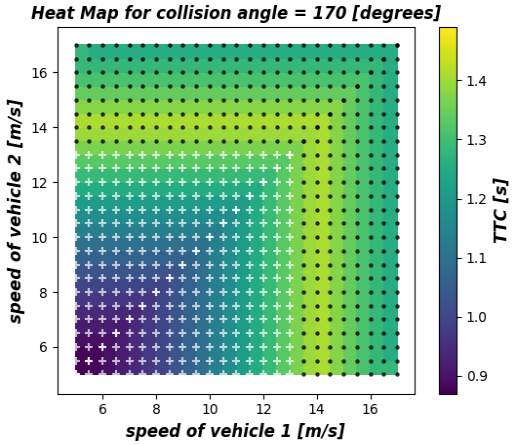
Heat Map for collision angle = 170 [degrees]
speed of vehicle 2 [m/s]
speed of vehicle 1 [m/s]
TTC [s]
6
8
10
12
14
16
0.9
1.0
1.1
1.2
1.3
1.4